Direct Dynamics for Free Radical Kinetics in Solution: Solvent Effect on the Rate Constant for the Reaction of Methanol with Atomic Hydrogen

5 AUTHORS, INCLUDING:

Yao-Yuan Chuang
National University of Kaohsiung
42 PUBLICATIONS   **1,333** CITATIONS

SEE PROFILE

Mala L Radhakrishnan
Wellesley College
24 PUBLICATIONS   **192** CITATIONS

SEE PROFILE

Christopher J Cramer
University of Minnesota Twin Cities
532 PUBLICATIONS   **23,458** CITATIONS

SEE PROFILE

Donald Truhlar
University of Minnesota Twin Cities
1,342 PUBLICATIONS   **81,416** CITATIONS

SEE PROFILE

Direct Dynamics for Free Radical Kinetics in Solution: Solvent Effect on the Rate Constant for the Reaction of Methanol with Atomic Hydrogen

Yao-Yuan Chuang, Mala L. Radhakrishnan, Patton L. Fast, Christopher J. Cramer, and Donald G. Truhlar*

Department of Chemistry and Supercomputer Institute, University of Minnesota, Minneapolis, Minnesota 55455-0431

Received: March 19, 1999; In Final Form: May 3, 1999

We calculate the rate constant for the reaction $^\bullet H + CH_3OH \rightarrow H_2 + {}^\bullet CH_2OH$ both in the gas phase and in aqueous solution at 298 K. To accomplish this, we apply two different methods to estimate the electronic energies along the reaction path. First, we use specific reaction parameters (SRP) to mix the exchange and correlation energies in Becke's adiabatic connection theory (AC-SRP) to optimize the model for the specific bond-breaking, bond-making combination under consideration. Second, we obtain the potential energy using a linear combination of the Hartree−Fock method and AM1 with specific reaction parameters (HF||AM1-SRP); in this linear mixing method, eight NDDO parameters and the linear mixing parameter are simultaneously optimized by a genetic algorithm. To calculate the reaction rate constants in solution, the solute atomic charges are represented by class IV charges, the electric polarization of the solvent is determined from the electronic charge distribution of the solute self-consistently, and the solute electronic, solvent electric polarization terms are augmented by first-solvation-shell terms calculated by the SM5.42 solvation model. Reaction rate constants of the hydrogen transfer reaction and the kinetic isotope effects are studied both in the gas phase at 200−2400 K and in aqueous solution at 298 K. The AC-SRP and HF||AM1-SRP methods, although quite different, give qualitatively similar pictures of the reaction at the separable equilibrium solvation level; however, it is found that a full equilibrium solvation path (ESP) calculation, which involves optimization of structures along the reaction path in the presence of solvent, is essential to reproduce the speedup of the reaction due to solvation. The final calculation, based on the HF||AM1-SRP electronic structure calculations and ESP dynamics with variational transition state theory in curvilinear coordinates with the microcanonical optimized multidimensional tunneling approximation, agrees well with experiment not only for the speedup due to the solvation but also for the $^\bullet D + CH_3OH$ and $^\bullet H + CD_3OH$ kinetic isotope effects.

1. Introduction

Recent years have seen great progress in modeling solvation effects on chemical reactions, especially ionic reactions[1−3] and polar rearrangements.[2−4] Radical chain reactions, in which a radical abstracts an atom from a molecule which is thereby converted to a radical, are an important class of reactions that has been less well studied.[5] Such bimolecular radical substitution (S_R2) reactions typically have smaller solvent effects than ionic reactions, and thus they provide a sensitive test of theory.

Mezyk and Bartels[6] have used pulse radiolysis (in which an electron beam is passed into the liquid to produce the $^\bullet H$ atoms) and EPR to determine the rate constant (k) of

$$^\bullet H + CH_3OH \rightarrow H_2 + {}^\bullet CH_2OH \qquad (1)$$
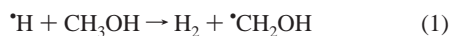
in aqueous solution, and since this reaction rate has been well studied in the gas phase, it provides an opportunity to test theories of radical kinetics in solution. Mezyk and Bartels fit their results to an Arrhenius expression that yields $k = 5.0 \times 10^{-15}$ cm^3 molecule^{-1} s^{-1} at 298 K.[6] They evaluated the rate enhancement compared to the gas phase as 23%, but we shall reanalyze the evidence for this in section 4.

A particularly intriguing question is whether there is a large hydrophobic acceleration due to association of the hydrophobic hydrogen atom with CH_3OH at the transition state. Mezyk and Bartels postulated that if a large hydrophobic acceleration is present, it must be largely canceled by liquid-phase quenching of the gas-phase tunneling contribution, since the net solvent effect is small.[6] It is important that any theoretical treatment aiming to resolve these effects and explain the solvent effect includes both tunneling and hydrophobic effects. The present treatment is based on variational transition state theory (VTST) with multidimensional tunneling (MT) contributions,[2,7−10] as extended in recent work on liquid-phase reactions.[11−14] (VTST/MT is also called semiclassical VTST or SC-VTST.) Solvation free energies are estimated by the SM5.42R[15] and SM5.42 solvation models, which include not only the hydrophobic effect but also electrostatic effects, dispersion, cavitation, and other effects of the perturbed solvent structure in the vicinity of the reacting solutes. The SM5.42R model is based on gas-phase geometries and gas-phase reaction paths, and the SM5.42 model[16] is obtained by relaxing these prescriptions (that is, by optimizing stationary point geometries and defining reaction coordiantes in the presence of solvent).

Section 2 presents the theoretical and computational methods and reports the results. Section 3 summarizes the experimental values. Section 4 presents a comparison of theory with experiment along with additional discussion, and section 5 offers concluding remarks.

2. Methods and Results

To calculate the reaction rate with VTST/MT in aqueous solution, we first adopt the separable equilibrium solvation (SES) approximation presented in a previous paper.[14] In the SES approximation, one first calculates a reaction path[17] (RP) in the gas phase and then solvates the system at geometries along the gas-phase RP (including reactants, products, and saddle point) by adding the standard-state molar free energy of solvation[18] to the gas-phase potential energy.

The canonical variational theory (CVT) rate constant at temperature T for a bimolecular reaction can be written as[11]

$$k^{\text{CVT}}(T) = \frac{\tilde{k}T}{hC^0} \exp\{-[G^0(\text{CVT}|T) - G^0(\text{R}|T)]/RT\} \quad (2)$$

where $\tilde{k}$ is Boltzmann's constant, R is the gas constant, h is Planck's constant, C^0 is the concentration corresponding to the standard state (taken here as 1 mol/L), $G^0(\text{R}|T)$ is the liquid-phase standard-state molar free energy (of activation) of reactants at temperature T, and $G^0(\text{CVT}|T)$ is the liquid-phase standard-state molar free energy of the canonical variational transition state at temperature T. The latter is given by

$$G^0(\text{CVT}|T) = \max_s G^0(\text{GT},s|T) \quad (3)$$

where $G^0(\text{GT},s|T)$ is the liquid-phase standard-state molar free energy at temperature T of a generalized transition state (GT) located at a value s of the reaction coordinate. In the SES approximation, the reaction coordinate s is taken as the signed distance from the gas-phase saddle point along the gas-phase minimum energy path in mass-scaled coordinates.[8,11] The standard-state free energy of the liquid-phase system is given by the sum of the Born–Oppenheimer potential energy $V(\mathbf{R}_\text{X})$ of the solute in the gas phase, the internal free energy of the solute molecule, $G_{\text{RVE}}(\text{X}|T)$, and the standard-state free energy of solvation $\Delta G_\text{S}^0(\mathbf{R}_\text{X}|T)$ with the same solute geometry, $\mathbf{R}_\text{X}$:

$$G^0(\text{X}|T) = V(\mathbf{R}_\text{X}) + G_{\text{RVE}}(\text{X}|T) + \Delta G_\text{S}^0(\mathbf{R}_\text{X}|T) \quad (4)$$

where X can be either reactants (R) or the generalized transition state (GT) at s. Note that the sum of the first and third term on the right-hand side of eq 4 is the potential of mean force[19] $W(\mathbf{R}_\text{X}|T)$; hence,

$$G^0(\text{X}|T) = W(\mathbf{R}_\text{X}) + G_{\text{RVE}}(T) \quad (5)$$

The reaction rate constants in aqueous solution are also calculated using the equilibrium solvation path (ESP) approximation. In this case, the geometries of the stationary points are optimized in the presence of solvent, and the reaction path is calculated using the potential of mean force, which is the sum of the gas-phase potential and the free energy of solvation, both considered as functions of all the degrees of freedom of the solute.

To calculate tunneling effects in either the SES or the ESP approximations, we employ the zero-order canonical mean shape (CMS-0) approximation[13] with the small-curvature tunneling (SCT) and large-curvature tunneling (LCT) approximations.[10] The SCT calculations are equivalent to tunneling along the reaction path with an effective potential and effective reduced mass. In the CMS-0 approximation, the effective potential for tunneling at temperature T is given by

$$V_{\text{eff}}(s) = V_{\text{eff,c}}(s) + G_{\text{RVE}}(s|T = 0) \quad (6)$$

where the classical effective potential is given by

$$V_{\text{eff,c}}(s) = V_{\text{RP}}(s) + \Delta G_\text{S}^0(s|T) \quad (7)$$

The effective reduced mass depends on the masses of the particles participating in the reaction coordinate and on the curvature of the reaction path in isoinertial coordinates. The LCT calculation involves both tunneling along the reaction coordinate and tunneling along paths that cannot be referred to the reaction coordinate; the latter follow straight-line cuts from the reactant valley to the product valley on the concave side of the curved reaction path in isoinertial coordinates. We recall that the most reliable estimate of the tunneling contributions is obtained by using the larger of the SCT and LCT tunneling probabilities at each total energy; this yields the microcanonical optimized multidimensional tunneling (μOMT) result.[10] The gas-phase reaction rate is calculated in the same way except with $\Delta G_\text{S}^0(s|T)$ set to zero.

To include the solvation effect along the reaction path completely, we would need to consider the nonequilibrium solvation (NES) effect, but the present work is limited to equilibrium solvation effects. The SES calculations involve the SM5.42R solvation models, and the ESP calculation involves SM5.42. All parameters of the SM5.42 model are taken to be the same as in the SM5.42R.

The electronic structure methods used here are partly empirical. An important methodological point, though, is that after the semiempirical parameters are determined, the gas-phase electronic energies, the solvation free energies, and the effective potentials used in the dynamics calculations and the dynamics calculations themselves are generated directly from electronic structure calculations of energies, energy gradients, energy Hessians, free energies, free energy gradients, and free energy Hessians without the intermediary of multidimensional fits to any of these quantities. Approaches that avoid global or semiglobal multidimensional fits of the potential energy function but instead obtain the required energies, gradients, and Hessians directly from electronic structure calculations are called direct dynamics.[9] For the present paper, all gradients were calculated analytically, and all Hessians were generated by finite differences of gradients.

Throughout this paper, the zero of potential energy V is chosen such that $V_{\text{RP}}(s = -\infty)$ equals zero.

2.1. Gas-Phase Reaction Path and Potential Surface. The first consideration is how many of the hydrogen atoms on the methanol molecule need to be considered for abstraction. The study of Lendvay et al.[20] indicates that abstracting the alcoholic hydrogen occurs with a much smaller rate than abstracting the methyl hydrogen because of its larger bond strength. Therefore, the alcoholic hydrogen abstraction is not considered in the present work. We note next that the three hydrogen atoms on the carbon are not all equivalent because they differ in the dihedral angles they make with the O–H hydrogen. Geometry optimization to search for a transition state in which the abstracted hydrogen atom makes a dihedral angle of 180° with the O–H hydrogen (the anti configuration) always results in a second-order saddle point, also called a hilltop, i.e., a stationary point with two imaginary frequencies. A first-order saddle point (a saddle point with one imaginary frequency) is found for abstracting either gauche hydrogen.

In reaction 1, a C–H bond is broken and an H–H bond is formed. Therefore, the classical energy of reaction is given by

$$\Delta E = D_\text{e}(\text{C–H}) - D_\text{e}(\text{H–H}) \quad (8)$$

Direct Dynamics for Free Radical Kinetics in Solution

J. Phys. Chem. A, Vol. 103, No. 25, 1999 **4895**

TABLE 1: Born–Oppenheimer Barrier Height ($V^{\ddagger}$), Energy of Reaction (ΔE), Bond Energies (D_e), and Saddle-Point Interatomic Distances ($R^{\ddagger}_{AB}$) Calculated with ab Initio Methods[a]

theory	$V^{\ddagger}$	ΔE	D_e(C–H)	D_e(H–H)	$R^{\ddagger}_{H-H}$	$R^{\ddagger}_{C-H}$
HF/6-31G*	21.7	−1.2	80.6	81.8	0.960	1.351
MP2/6-31G*	20.2	2.4	95.1	92.7	0.928	1.373
QCISD/6-31G*	16.6	−2.1	95.3	97.4	0.963	1.358
HF/cc-pVDZ	19.8	−2.7	79.0	81.7	0.972	1.346
MP2/cc-pVDZ	14.4	−1.0	97.3	98.3	0.941	1.355
QCISD/cc-pVDZ	10.5	−5.7	97.9	103.6	0.984	1.326
CCSD/cc-pVDZ	10.8	−5.5	98.1	103.6	0.980	1.328
HF/cc-pVTZ	20.1	−4.1	79.6	83.7	0.967	1.334
MP2/cc-pVTZ	14.3	−1.9	101.7	103.6	0.928	1.342

[a] This table contains only gas-phase quantities. The energies exclude zero-point contributions and are in kcal/mol; bond lengths are in angstroms. The bond distances shown in Tables 1, 2, and 4 are those for the making and breaking bonds.

where D_e(A–B) is the equilibrium dissociation energy of the A–B bond. Bauschlicher et al.[21] calculated the equilibrium C–H bond energy of methanol to be 102.4 kcal/mol using a modified coupled-pair functional (MCPF) approach; applying a correction of 2 kcal/mol, they then estimated the equilibrium C–H bond energy to be 104.4 kcal/mol in the complete CI limit. The H–H equilibrium bond energy is 109.5 kcal/mol, as calculated by Kolos and Wolniewicz.[22] We use these values to estimate the zero-point-exclusive energy of the reaction (ΔE) to be −5.1 kcal/mol.

We then estimate the classical (i.e., the zero-point-exclusive) gas-phase barrier height $V^{\ddagger}$ based on the experimental activation energy. Tsang's evaluation[23] of the experimental data leads to a temperature-dependent Arrhenius activation energy of

$$E_a = (2450\ K)R + 2.11RT \tag{9}$$

where K denotes a Kelvin, R is the gas constant, and T is temperature. This leads to a phenomenological energy of activation of 7–11 kcal/mol over the temperature range 500–2000 K. In our experience with reactions studied previously, a very rough estimate of the classical barrier height is E_a(800 K) $\pm$ 2 kcal/mol, which yields 8 $\pm$ 2 kcal/mol. Lendvay et al.[20] obtained slightly higher values, 11.34 and 10.55 kcal/mol, from bond-addivity-corrected Møller–Plesset fourth-order perturbation theory[24] (BAC-MP4) and from the Gaussian-2 method[25] (G2), respectively. From Table 1, we notice that other ab initio methods also predict too high a barrier height, ranging from 10.5 to 22 kcal/mol. (One result of the present dynamics calculations, which will employ a classical barrier height of ∼8 kcal/mol, will be to allow us to make a better determination of what value (or range of values) of $V^{\ddagger}$ is most consistent with existing experiments. We will return to this question in section 4.1.)

To carry out an accurate dynamics calculation, it is required to find a level of electronic structure theory that gives an accurate barrier height ($V^{\ddagger}$) and Born–Oppenheimer energy of reaction (ΔE). We examined several ab initio methods, including Hartree–Fock theory,[26] second-order Møller–Plesset perturbation theory[27] (MP2), quadratic configuration interaction based on single and double excitations[28] (QCISD), and the coupled-cluster method with single and double excitations[29] (CCSD). We also employed several density functional theory[30] (DFT) methods and hybrid Hartree–Fock/density functional theory methods based on Becke's three-parameter adiabatic connection[31–33] method. (Becke uses density functional theory plus an adiabatic connection to develop an admixture of Hartree–

TABLE 2: Born–Oppenheimer Barrier Height ($V^{\ddagger}$), Energy of Reaction (ΔE), Bond Energies (D_e), and Saddle-Point Interatomic Distances ($R^{\ddagger}_{AB}$) Calculated with Density Functional Theory and Adiabatic Connection Methods[a]

theory	$V^{\ddagger}$	ΔE	D_e(C–H)	D_e(H–H)	$R^{\ddagger}_{H-H}$	$R^{\ddagger}_{C-H}$
B3LYP/MIDI!	1.7	−9.8	97.9	107.7	1.070	1.261
B3LYP/6-31G*	3.6	−8.1	101.7	109.8	1.011	1.301
B3PW91/6-31G*	5.0	−6.2	100.7	106.8	1.001	1.307
B3P86/cc-pVDZ	1.1	−8.2	101.5	109.7	1.027	1.298
B3LYP/cc-pVDZ	2.0	−8.6	98.8	107.4	1.026	1.299
B3PW91/cc-pVDZ	3.3	−6.9	98.2	105.1	1.031	1.285
best estimate	6–10	−5.1	104.4	109.5		

[a] This table contains only gas-phase quantities. The energies exclude zero-point contributions and are in kcal/mol; bond lengths are in angstroms. The bond distances shown in Tables 1, 2, and 4 are those for the making and breaking bonds.

Fock, local density functional, and nonlocal density functional approximations to the Fock–Kohn–Sham operator. This provides an alternative to the MP2, QCISD, and CCSD approaches for the inclusion of electron exchange and electron correlation.) For these methods, the MIDI!,[34] 6-31G*,[35] correlation-consistent polarized valence double-ζ[36] (cc-pVDZ), and correlation-consistent polarized valence triple-ζ[37] (cc-pVTZ) basis sets were used. None of the "pure" methods gives a good approximation to the classical barrier height and the energy of the reaction. We then carried out the reaction rate constant calculations using two new approximations to estimate the free energy profiles and the other information required along the reaction path and tunneling paths. The first approximation is based on a new set of parameters for Becke's adiabatic connection method. The second approximation is based on a linear combination of ab initio Hartree–Fock and semiempirical AM1 theories. These new methods are explained in the next two sections.

2.1.1. Adiabatic Connection Method with Specific Reaction Parameters (AC-SRP). Table 2 gives energetic and geometric information from several AC calculations. We see that one of the methods (i.e., B3PW91/6-31G*) predicts $V^{\ddagger}$ and ΔE values close to our estimates of 8 and −5 kcal/mol, respectively. We therefore took this as a starting point for improvement. To improve the AC potential energy surface for reaction 1, we developed a semiempirical strategy that we will call AC-SRP to denote using specific reaction parameters (SRP) in the AC method. In particular, we use Becke's three-parameter (B3) exchange-correlation operator, which is given by

$$F_{AC} = A F_X^{Slater} + (1 - A) F_X^{HF} + B \Delta F_X^{Becke} + C \Delta F_C^{PW91(NL)} + F_C^{PW91(L)} \tag{10}$$

where F_X^{Slater} is the Slater local exchange functional,[37] F_X^{HF} is the nonlocal exchange energy operator of Hartree–Fock theory, ΔF_X^{Becke} is Becke's 1988 gradient correction[38] to Slater's exchange functional, and $\Delta F_C^{PW91(NL)}$ and $F_C^{PW91(L)}$ are the Perdew–Wang 1991[39] nonlocal and local correlation energy functionals, respectively. The optimized values of A, B, and C suggested by Becke are 0.8, 0.72, and 0.81, respectively.[31] These values were optimized in an average way for a small training set of experimental thermochemical data. For a specific reaction, however, these parameters may not be optimum. For reaction 1, the barrier height ($V^{\ddagger}$) varied inversely with A and C and directly with B, while ΔE varied directly with A and C and inversely with B. Therefore, because the B3PW91/6-31G* values of both $V^{\ddagger}$ and ΔE are lower than the desired values, more than one parameter needs adjustment to obtain agreement with experiment. After extensive experimentation, we concluded

TABLE 3: Specific Reaction Parameters for Both AC-SRP and HF||AM1-SRP Methods

		original	AC-SRP[a]	HF||AM1-SRP[a]
A		0.80	0.60 (25)	
B		0.72	0.50 (31)	
C		0.81	0.81	
U_{SS}	C	−52.029		−49.851 (4.2)
U_{PP}	C	−39.614		−40.337 (1.8)
U_{SS}	O	−97.830		−99.182 (1.4)
U_{PP}	O	−78.262		−80.763 (3.2)
β_S	C	−15.716		−16.913 (9.7)
β_P	C	−7.719		−9.190 (19)
β_S	O	−29.273		−28.998 (0.9)
β_P	O	−29.273		−29.249 (0.1)
x^b				0.244

[a] Number in parentheses is absolute percent change from the original value. [b] Mixing parameter of eq 11.

TABLE 4: Born−Oppenheimer Barrier Height ($V^{\ddagger}$), Energy of Reaction (ΔE), Bond Energies (D_e), and Saddle-Point Interatomic Distances ($R^{\ddagger}_{AB}$) Calculated with Various Electronic Structure Methods[a]

theory	$V^{\ddagger}$	ΔE	D_e(C−H)	D_e(H−H)	$R^{\ddagger}_{H-H}$	$R^{\ddagger}_{C-H}$
B3PW91/6-31G*	5.0	−6.2	100.7	106.8	1.001	1.308
AC-SRP	7.8	−4.5	101.4	106.0	0.971	1.322
HF/STO-3G	19.1	−11.2	104.5	115.7	0.968	1.275
AM1	−0.4	−28.0	81.4	109.4	1.341	1.135
AM1-SRP	4.1	−4.9	104.4	109.3	0.804	1.310
HF||AM1-SRP[b]	7.8	−5.0	105.6	110.7	0.867	1.277
best estimate	8−10[c]	−5.1	104.4	109.5		

[a] This table contains only gas-phase quantities. The energies exclude zero-point contributions and are in kcal/mol; bond lengths are in angstroms. The bond distances shown in Tables 1, 2, and 4 are those for the making and breaking bonds. [b] In this paper, HF||AM1-SRP denotes HF/STO-3G||AM1-SRP. [c] See section 4.1.

(as have others before us) that the results are much more sensitive to A and B than to C. Therefore, we will concentrate on A and B and adjust them in order to obtain better agreement with experiment for the specific reaction 1. The results obtained with specifically adjusted parameters will be called AC-SRP. For reaction 1, we varied A and B to find values that produce reasonably accurate values for $V^{\ddagger}$ and ΔE without significantly degrading the original AC predictions of the C−H and H−H bond strengths and transition state bond lengths. The first three rows of Table 3 show the standard values of A, B, and C and also the specific adjusted values used in this work; the latter are in the row labeled AC-SRP. We found that the combination $A = 0.6$ and $B = 0.5$ provides acceptable values for $V^{\ddagger}$ and ΔE as well as reasonable bond energies and geometries as shown in Table 4.

With this approach, the optimized transition state geometry has a dihedral angle of ∼72° between the abstracted hydrogen atom and the alcoholic hydrogen atom (the gauche or skew configuration). Changing the dihedral angle corresponds to rotating the alcoholic hydrogen atom around the C−O bond. We optimized geometries at three stationary points corresponding to local minima or maxima along this coordinate. One, at the anti configuration, has a barrier height of 4.2 kcal/mol (relative to the skew case as shown in Figure 1), and the other, at the eclipsed configuration (where the alcoholic hydrogen atom has a dihedral angle of 0° with respect to the abstracted hydrogen atom), has a barrier height of 3.3 kcal/mol. Both of these barriers are higher than the barrier of 2.2 kcal/mol calculated for methanol using the same combination of the parameters A, B, and C; this means that the 72° structure is the lowest energy saddle point between reactants and products.
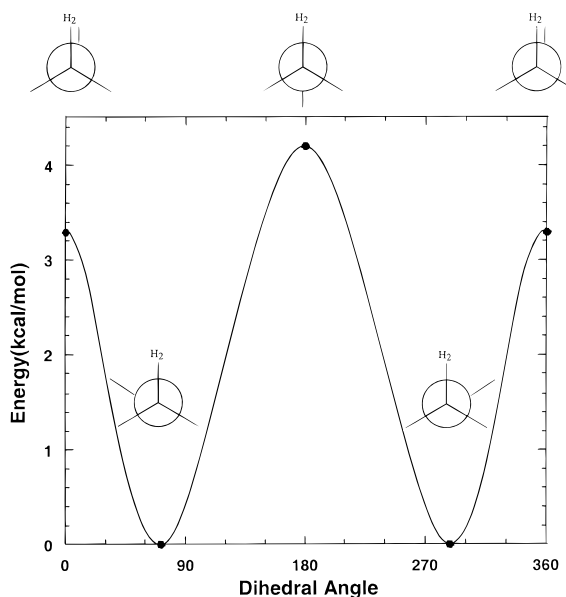
Figure 1. Spline fit to saddle-point and hilltop energies in the gas phase as a function of the H−C−O−H dihedral angle from AC-SRP calculations. For this figure, the zero of energy is at the saddle point.

We then estimated the reduced moments of inertia for internal rotation by the method of Pitzer;[40,41] and we used these with a formula presented previously[42] to calculate hindered rotation partition functions for both methanol molecule and the transition state. For methanol, the hindered rotation partition function at 2000 K is estimated to be 3.50 as compared to the harmonic limit of 3.97 (a deviation of 12%). Using the same approach for the saddle point, the deviation is only 7% at 2000 K. At lower temperatures, the deviation from the harmonic approximation is smaller, and at room temperature, the harmonic oscillator approximation is adequate. Therefore, all further calculations are based on the harmonic-oscillator/rigid-rotor[43] approximations.

2.1.2. Linear Combination of Hartree−Fock and Molecular Orbital Method (HF||AM1-SRP). Even though the AC-SRP method seems to provide a reasonable potential energy surface and has reasonable computational cost for gas-phase calculations at stationary points, there are two disadvantages in this method: (1) it is computationally costly to follow the whole reaction path or to carry out LCT calculations; (2) the analytical gradient of the solvation free energy is not yet implemented for the Becke three-parameter method. Therefore, we will only use the AC-SRP method for gas-phase and SES calculations. We next describe a less expensive procedure for obtaining an SRP potential energy surface that will be used to examine the sensitivity of the SES result to the parametization method and to study the difference between SES and ESP calculations. The new method, to be called HF||AM1-SRP, should be especially useful for calculations on large molecules. The HF||AM1-SRP method also makes LCT calculations more affordable (recall that LCT calculations require more input than SCT calculations[10]).

The HF||AM1-SRP method involves a linear combination of total electronic energies from the Hartree−Fock and from semiempirical molecular orbital theory (in this case AM1[44]) with specific reaction parameters. Note that AM1 with specific reaction parameters (AM1-SRP) is a special case of the NDDO-

Direct Dynamics for Free Radical Kinetics in Solution

J. Phys. Chem. A, Vol. 103, No. 25, 1999 **4897**

SRP method.[45] The total electronic energy is written as

$$E_{HF||AM1-SRP} = xE_{HF} + (1-x)E_{AM1-SRP} \qquad (11)$$

where x is the mixing parameter, E_{HF} is the electronic energy from Hartree−Fock theory, and $E_{AM1-SRP}$ is the electronic energy from the AM1-SRP Hamiltonian. Equation 11 differs in a fundamental way from eq 10. Equation 11 involves a linear combination of separately calculated energies rather than a combination of operators and functionals as in (10). To implement eq 10 requires mixing theories at the level of the Fock−Kohn−Sham operator, whereas eq 11 can be implemented more modularly by combining separate energy calculations. Furthermore, the analytic gradient of eq 11 is easily implemented as the sum of the analytic gradients of the two terms on the right-hand side, and this analytic gradient is used for optimizing geometries and calculating reaction paths. The general approach in eq 11, by which two or more energy components are combined linearly with a coefficient optimized for a specific reaction (or specific limited range of systems), is called linear mixing with specific reaction parameters (LM-SRP). In the present application, we also add additional specific reaction parameters in one of the two energy components, namely the AM1 component, in which we will optimize eight parameters simultaneously with x. This specific implementation of LM-SRP is called HF||AM1-SRP.

To test whether useful results can be obtained by the HF||AM1-SRP method with minimal expense, we use the STO-3G[46] minimal basis set for the HF calculations. Table 3 shows the value of x and the changed AM1-SRP parameters that reproduce the $V^{\ddagger}$ and ΔE calculated from the AC-SRP method. These parameters (x and the eight other parameters in the last column of Table 3) were determined by using a genetic algorithm[47] (GA). The pure HF/STO-3G results, the unmodified AM1 results, and the unmixed AM1-SRP results are also shown in Table 4. It is important to point out that the NDDO parameters of the AM1-SRP method were optimized with nonzero x; that is, they were optimized simultaneously with x by the GA to make $E_{HF||AM1-SRP}$ agree well with the AC-SRP results rather than to make the $E_{AM1-SRP}$ term useful on its own. (We found in earlier calculations that the AM1-SRP method with $x = 0$ did not give as good a potential surface as those considered here.) We note that Hartree−Fock theory has the tendency to overestimate classical barrier heights ($V^{\ddagger}$) due to the lack to electron correlation. We also note that pure AM1 calculations often provide quite inaccurate geometries for saddle points. The purpose of the linear combination method is to allow one to obtain reasonable results for a specific reaction at low computational cost and at the same time allow us include a convenient starting point for calculations on liquid-phase solutions.

In a certain sense, the HF||AM1-SRP strategy works for the same reasons that Becke's original B3 strategy works. In particular, the B3 strategy mixes an ab initio Hartree−Fock calculation, which tends to overestimate barrier heights and underestimate bond energies, with a DFT component, and pure DFT tends to underestimate[32] barrier heights. The HF||AM1-SRP method reduces the cost and complexity of this successful strategy in three ways: (i) a very small basis set is used for the HF component (barrier heights are still overestimated by HF theory, even with small basis sets); (ii) AM1-SRP is substituted for DFT; (iii) the theories are mixed at the energy level rather than the Fock-operator level.

As for the AC-SRP case, all further calculations with HF||AM1-SRP are based on the harmonic oscillator and rigid-rotor[43] approximation.

2.2. Validation of the Gas-Phase Charge Distribution and Dipole Moment. To make the dynamics calculations in solution credible, we also need to validate the accuracy of the electronic charge distribution in the gas phase. The reason for this is that the charge distribution is a major factor in determining the electrostatic portion of the solvation free energy; thus, if the gas-phase charge distribution were inaccurate, the calculations might give unreliable solvation free energies. It has been shown previously that accurate charge distributions can be obtained from HF, B3PW91, B3LYP, and AM1 wave functions by Charge Model 2[48] (CM2), which involves a class IV mapping,[49] and the SM5.42R[15] and SM5.42[16] solvation models use these charges. The present situation, though, is subtle insofar as the solvation free energies are calculated by the CM2 and SM5.42R models, which are parametrized for (among others) BPW91/6-31G*, B3LYP/MIDI!, HF/MIDI!, and AM1 but not for AC-SRP, HF/STO-3G, or AM1-SRP. In the SM5.42[15] or SM5.42R[16] solvation models, the cavity dispersion solvent structure (CDS) terms must be consistent with a *given* treatment of the electrostatics. We use experimental and original-parameter CM2 dipole moments and original-parameter CM2 partial charges as diagnostics of the accuracy of the partial charges. We also performed additional ab initio calculations to test the charge distribution.

2.2.1. Charges and Dipole Moments in AC-SRP. Calculating accurate partial atomic charges at points along the reaction path is essential to calculating accurate rate constants of reactions in liquid-phase solutions. The CM2 charge model is a semiempirical class IV charge model that has been parametrized for several basis sets and levels of treatment of the electronic wave function. Although it has not been parametrized for AC-SRP/6-31G*, it has been parametrized for the standard BPW91/6-31G* method. We employed the charge model parameters intended for the BPW91/6-31G* method with the adjusted AC-SRP/6-31G* method and determined whether the resulting calculated charges and dipole moments are within an acceptable range as judged by experiment and high-level theory for reactants and products. The gas-phase dipoles and partial atomic charges for CH_3OH and CH_2OH calculated from various ab initio methods and density functional models are compared to our values from AC-SRP calculations in Table 5. Because the AC-SRP values of the dipole moments and partial charges on our molecule are within the error of experiment and of the CM2 charges calculated with the original globally validated[48] parameters and are also reasonably close to other theoretical values, we concluded that a readjustment of charge model parameters is not required.

Because we will use SM5.42R solvation parameters originally determined[15] for the BPW91/6-31G* method, it is important not only that the AC-SRP/6-31G* gas-phase charge distribution is reasonably accurate but also that it does not differ significantly from the BPW91/6-31G* charge distribution. Table 5 also confirms that this test is satisfied.

2.2.2. Charges and Dipole Moments in HF||AM1-SRP. We also need to check and validate the charge distribution of the HF||AM1-SRP method. Since there are no CM2 parameter sets optimized for the HF/STO-3G and AM1-SRP methods, new CM2 parameter sets are required. In the spirit of specific reaction parameters[45,50] (SRP), we denote the new parametrized procedure as CM2-SRP. Similarly to the standard procedure used to determine the C and D parameters for the CM2 charge model,[48] we first fixed the partial charge of benzene at 0.11 by setting the C_{C-H} parameter, then the rest of the parameters were determined by fitting to the partial charges of the methanol and

TABLE 5: Dipole Moments of CH₂OH and CH₃OH

level[a]	method[b]	dipole moment (D)
	CH₃OH	
HF/MIDI!	CM2/HF/MIDI!	1.63
HF/MIDI!6D//HF/MIDI!	CM2/HF/MIDI!6D	1.62
HF/6-31G*//HF/MIDI!	CM2/HF/6-31G*	1.69
BPW91/MIDI!// HF/MIDI!	CM2/BPW91/MIDI!	1.65
B3LYP/MIDI!// HF/MIDI!	CM2/B3LYP/MIDI!	1.63
BPW91/6-31G*// HF/MIDI!	CM2/BPW91/6-31G*	1.71
BPW91/6-31G*	CM2/BPW91/6-31G*	1.62
AC-SRP/6-31G*	CM2/BPW91/6-31G*	1.74
experimental		1.7
	CH₂OH	
MP2/6-31G*//AC- SRP/6-31G*	ChelpG	1.57
MP2/cc-pVDZ//AC- SRP/6-31G*	ChelpG	1.42
QCISD/cc-pVDZ	ChelpG	1.44
MP2/cc-pVDZ	ChelpG	1.45
B3LYP-SRP/MIDI!//AC- SRP/6-31G*	CM2/B3LYP/MIDI!	1.39
BPW91/MIDI!//AC- SRP/6-31G*	CM2/BPW91/MIDI!	1.38
BPW91/6-31G*//AC- SRP/6-31G*	CM2/BPW91/6-31G*	1.43
AC-SRP/6-31G*	CM2/BPW91/6-31G*	1.49

[a] In B3LYP-SRP, the LYP nonlocal functional is substituted for the PW91 nonlocal functional in the standard way (ref 58) but with the AC-SRP values of *A*, *B*, and *C*. [b] In each case, this column gives the method that is used to calculate partial atomic charges and the dipole moment is calculated from these charges.

TABLE 6: CM2-SRP Parameters

	C_{H-C}	C_{H-O}	C_{C-O}	D_{C-O}
AM1[a]	−0.0200	0.1770	0.0260	0.0160
CM2-AM1-SRP[b]	−0.0200	0.0149	−0.0874	0.0215
CM2-STO-3G[c]	−0.0210	0.2953	−0.0111	−0.0068

[a] Original CM2 parameter set for AM1 wave function. [b] CM2-SRP parameter set for AM1-SRP wave function. [c] CM2-SRP parameter set for HF/STO-3G wave function.

TABLE 7: Gas-Phase Dipole Moment in Debyes with Geometries Optimized by HF||AM1-SRP[a]

wave function	CM2 parameters	CH₃OH	CH₂OH	CH₄OH
AM1	AM1	1.63	1.43	1.44
AM1-SRP	AM1	2.48	2.15	2.30
HF/STO-3G	AM1	1.29	1.27	1.13
AM1-SRP	CM2-AM1-SRP	1.73	1.45	1.58
HF/STO-3G	CM2-STO-3G	1.67	1.81	1.63
HF||AM1-SRP[a]	CM2-AM1-SRP|| CM2-STO-3G	1.64	1.49	1.48

[a] HF||AM1-SRP means HF/STO-3G||AM1-SRP. For this method, the tabulated dipole moment is calculated by eq 12.

hydroxymethyl radical using a genetic algorithm[47] (GA). The CM2-SRP parameters are given in Table 6, and the dipole moments are shown in Table 7. The dipole moment of the HF||AM1-SRP method is determined by assuming the partial charges are scaled in the same way as the electronic energies. Therefore,

$$q_{HF||AM1-SRP} = xq_{HF} + (1 - x)q_{AM1-SRP} \quad (12)$$

where x is the mixing parameter, q_{HF} is the partial charge calculated by HF/STO-3G using the CM2-SRP charge model, and $q_{AM1-SRP}$ is the partial charge calculated by AM1-SRP using

TABLE 8: ΔG_{EP}, ΔG_{CDS}, and Free Energy of Solvation ΔG_S^0 of the Atoms in Reactants, Products, and Saddle Point Using the SES Approximation with Geometries Optimized in the Gas Phase by AC-SRP

	reactants			saddle point			products		
atom[a]	ΔG_{EP}	G_{CDS}	ΔG_S^0	ΔG_{EP}	G_{CDS}	ΔG_S^0	ΔG_{EP}	G_{CDS}	ΔG_S^0
H	0.00	1.80	1.80	−0.80	1.26	0.46	0.00	1.18	1.18
X	0.01	0.04	0.05	0.12	0.09	0.21	0.00	1.18	1.18
C	0.05	1.21	1.27	0.13	1.20	1.33	−0.10	1.74	1.64
O	−2.00	−2.53	−4.53	−0.13	−2.00	−2.13	−0.72	−1.78	−2.50
Y	−0.28	0.04	−0.24	−0.55	0.04	−0.51	0.16	0.04	0.20
Z	−0.28	0.04	−0.24	−0.13	0.04	−0.09	−0.30	0.04	−0.26
W	−1.67	−0.35	−2.02	−3.11	−0.35	−3.46	−3.02	−0.35	−3.37
sum	−4.17	0.25	−3.91	−4.47	0.28	−4.19	−3.98	2.05	−1.93
Δ(sum)[b]	0.00	0.00	0.00	−0.30	0.03	−0.28	0.19	1.80	1.98

[a] To distinguish the hydrogen atoms, the symbols X, Y, Z, and W are used. The reaction is described as H + XCYZOW → XH + CYZOW. [b] Difference with respect to the values at reactants.

the CM2-SRP charge model. We find that the partial charges calculated using this linear combination with the adjusted CM2 parameters are close to the values of the globally validated CM2/AM1 method. Since the dipole moments are very similar to the CM2/AM1 ones, we use the AM1 solvation parameters for the SM5.42 calculations based on the HF||AM1-SRP description.

2.3. Solvation Free Energies. Having checked and validated the gas-phase charge distributions against gas-phase dipole moments, we used the SM5.42R and SM5.42 models to calculate the free energies of solvation. Note that this involves adding the solvent reaction field to the mixed Fock operator of AC-SRP theory and to each Fock operator of the LM-SRP theory (i.e., separately to the HF and AM1-SRP Fock operators). Furthermore, the linear mixing of energy components in LM-SRP theory becomes a linear combination of potentials of mean force. We remind the reader that SM5.42R theory uses a geometry optimized in the gas phase while SM5.42 theory involves geometry optimization in the liquid phase. Thus, the SM5.42R/AC-SRP calculations involve an AC-SRP gas-phase geometry, and the SM5.42R/HF//AM1-SRP calculations involve an HF||AM1-SRP gas-phase geometry.

The solute-electronic and solvent-polarization contribution (ΔG_{EP}) to free energy of solvation, the cavitation dispersion solvent structure contributions (G_{CDS}) to free energy of solvation, and the total free energy of solvation (ΔG_S^0) of the reactants, products, and saddle point calculated by the SM5.42R/AC-SRP method are given in the sum row of Table 8. Recall that ΔG_{EP} consists of two terms:

$$\Delta G_{EP} = \Delta E_E + G_P \quad (13)$$

[15] where G_P is the electric polarization free energy of the solvent, including the solvent reorganization cost, as estimated by the generalized Born approximation, and ΔE_E is the solute electronic distortion cost that is incurred in achieving the self-consistent polarization field. We note that

$$G_P = \left(\frac{1 - \epsilon}{2\epsilon}\right) \sum_k \sum_{k'} q_k q_{k'} \gamma_{kk'} \quad (14)$$

where ϵ is the solvent's dielectric constant, q_k is the self-consistent partial charge on atom k, and $\gamma_{kk'}$ is a Coulomb integral. For the higher rows in Table 8, the ΔG_{EP} values are

Direct Dynamics for Free Radical Kinetics in Solution

J. Phys. Chem. A, Vol. 103, No. 25, 1999 **4899**

TABLE 9: ΔG_{EP}, ΔG_{CDS}, and Free Energy of Solvation ΔG_S^0 of the Atoms in Reactants, Products, and Saddle Point at HF||AM1-SRP Using the SES Approximation with Geometries Optimized in the Gas Phase by HF||AM1-SRP

atom[a]	reactants			saddle point			products		
	ΔG_{EP}	G_{CDS}	ΔG_S^0	ΔG_{EP}	G_{CDS}	ΔG_S^0	ΔG_{EP}	G_{CDS}	ΔG_S^0
H	0.00	1.80	1.80	−0.02	1.23	1.21	0.00	1.16	1.16
X	−0.01	−0.02	−0.03	−0.28	0.04	−0.24	0.00	1.16	1.16
C	0.03	1.34	1.37	0.06	1.33	1.39	−0.07	1.92	1.85
O	−1.80	−2.09	−3.88	−1.20	−1.76	−2.96	−0.66	−1.16	−1.82
Y	−0.22	−0.02	−0.24	−0.28	−0.02	−0.30	0.11	−0.18	−0.07
Z	−0.22	−0.02	−0.24	−0.01	−0.02	−0.03	−0.28	−0.03	−0.32
W	−2.26	−0.65	−2.92	−2.77	−0.66	−3.44	−3.55	−0.50	−4.06
sum	−4.47	0.34	−4.13	−4.51	0.13	−4.38	−4.46	2.36	−2.10
Δ(sum)[b]	0.00	0.00	0.00	−0.04	−0.20	−0.24	0.01	2.02	2.04

[a] To distinguish the hydrogen atoms, the symbols X,Y, Z, and W are used. The reaction is described as H + XCYZOW → XH + CYZOW. [b] Difference with respect to the values at reactants.

partitioned among the atoms k based on the following expression:

$$\Delta G_{EP}(k) = \Delta G_{EP} \frac{G_P(k)}{\sum_k G_P(k)} \quad (15)$$

where $G_P(k)$ is defined in a previous paper.[51] Equation 15 has the desirable property that the total electronic and polarization contribution to the solvation free energy is the sum of a contribution $\Delta G_{EP}(k)$ from each atom.

$$\Delta G_{EP} = \sum_k \Delta G_{EP}(k) \quad (16)$$

The CDS contributions are also partitioned among atoms; this partitioning is more obvious since the CDS term is easily written as a sum of terms each associated with the surface area of a given atom.[15,52] The total free energies of solvation obtained from the HF||AM1-SRP calculations are tabulated in Tables 9 and 10 for the SES and ESP approximations.

In the ESP calculation, the geometries of the stationary points are reoptimized in solution. While one can still tabulate and analyze ΔG_{EP}, it is also instructive to consider the contribution from changing the geometry. This converts ΔG_{EP} to ΔG_{ENP} where N denotes the nuclear part. Note that

$$\Delta G_S^0(\text{SM5.42R}) = \Delta G_{EP} + G_{CDS} \quad (17)$$

and

$$\Delta G_S^0(\text{SM5.42}) = \Delta G_{ENP} + G_{CDS} \quad (18)$$

All three calculations indicate an increase of the positive value of G_{CDS} as the reaction moves to the product side, and this contributes to decreasing the equilibrium constant in aqueous solution as compared to the gas phase.

2.4. Saddle Point Geometries. Table 11 gives the valence internal coordinates for the three saddle-point structures used for the dynamics calculations reported here.

2.5. Dynamics. *2.5.1. AC-SRP.* All reaction path calculations were carried out in isoinertial coordinates[8] scaled to a reduced mass μ of 1.0 amu. Although we developed the interpolated variational transition state theory by mapping[53] (IVTST-M) algorithm to allow us to obtain reasonable reaction rates by using VTST/SCT with reaction paths covering a very limited range

of reaction path, in the present work, since it is a qualitatively new kind of application and since we wish to carry out μOMT calculations as consistently as possible with SCT ones, we decided to follow the reaction path over a wide range in the reaction coordinate to prevent any possible imprecision that might be introduced by the interpolation scheme. First, we calculated the gas-phase reaction path using the Page−McIver[54] method. The gradient step size was 0.0026 Å, and Hessians were calculated at every second gradient point from −1.3 to 0.8 Å along the reaction coordinate. The vibrational frequencies along the reaction path were evaluated using a set of redundant internal coordinates[55] that consist of six stretches, seven nondegenerate bends, one doubly degenerate linear bend, and two torsions. The lowest real frequency mode of methanol and the generalized transition states corresponds to the internal rotation of the alcoholic hydrogen atom around the C−O bond and can be treated with the hindered rotator approximation,[40−42] but as discussed above, we used the harmonic treatment due to the small anharmonicity. The forward symmetry factor is set to 2.

The tunneling calculation was carried out with the small-curvature tunneling approximation[10] (SCT) with 40 coordinate points for each action integral and was Boltzmann averaged using 40 energies. The effective reduced mass[10] is interpolated along the reaction path using a sixth-order Lagrangian interpolation scheme. The final gas-phase rate constants calculated are given in Table 12, where they are compared with the experimental values.

To include the free energy of solvation along the gas-phase reaction path for the separable equilibrium solvation (SES) approximation, we used variational transition state theory with the interpolation based on single-point energies algorithm[56] (VTST-ISPE).

Figure 2 shows a plot of

$$\Delta V_{eff,c}(s) = V_{eff,c}(s) - V_{eff,c}(s = \text{reactants}) \quad (19)$$

for both the gas-phase and the aqueous-phase versions of reaction 1 as calculated by the AC-SRP method.

2.5.2. HF||AM1-SRP. The dynamics calculations with the HF||AM1-SRP method are also carried out with a scaling mass equal to 1.0 amu. The reaction path was followed using the Page−McIver[54] method in the range −0.8 to 0.8 Å with a gradient step size of 0.0011 Å. The harmonic vibrational frequencies were calculated using redundant internal coordinates[55] at every fourth gradient step. The small-curvature tunneling[10] (SCT) calculation is again carried out with 40 coordinate points for each action integral and Boltzmann averaged using 40 energies. The effective reduced mass for SCT is interpolated using a sixth-order Lagrangian interpolation scheme. For the HF||AM1-SRP calculations, large-curvature tunneling[10] (LCT) calculations were also carried out. All excited states are included for LCT calculations (as described in ref 10) if they are allowed. The reaction rate constants in liquid-phase solution are estimated using both the SES and ESP methods, and all dynamical calculations in solution were carried out with the same numerical parameters as in the gas phase. To check the stability of the calculations with respect to reorienting the generalized transition state dividing surfaces, all HF||AM1-SRP calculations were repeated with the RODS[57] algorithm. The average change in the rate constants at 298 K was 1% for gas-phase rates, 5% for SES, and 9% for ESP. These changes are small enough not to affect our conclusions, so for consistency with the AC-SRP calculations, we report the results obtained without RODS.

TABLE 10: ΔG_{EP}, ΔG_{CDS}, and Free Energy of Solvation ΔG_S^0 of the Atoms in Reactants, Products, and Saddle Point at HF||AM1-SRP Using the ESP Approximation with Geometries Optimized in Water by SM5.42/HF||AM1-SRP

	reactants			saddle point			products		
atom[a]	ΔG_{EP}	G_{CDS}	$\Delta G_{EP} + G_{CDS}$	ΔG_{EP}	G_{CDS}	$\Delta G_{EP} + G_{CDS}$	ΔG_{EP}	G_{CDS}	$\Delta G_{EP} + G_{CDS}$
H	0.00	1.80	1.80	−0.02	1.22	1.20	0.00	1.16	1.16
X	0.00	−0.02	−0.02	−0.28	0.04	−0.24	0.00	1.16	1.16
C	0.03	1.34	1.37	0.06	1.34	1.40	−0.10	1.92	1.82
O	−1.83	−2.09	−3.93	−1.28	−1.94	−3.22	−0.68	−1.16	−1.83
Y	−0.21	−0.02	−0.23	−0.31	−0.02	−0.33	0.13	−0.03	0.10
Z	−0.21	−0.02	−0.23	0.00	−0.02	−0.03	−0.30	−0.03	−0.33
W	−2.34	−0.66	−2.99	−2.87	−0.66	−3.53	−3.75	−0.66	−4.41
sum	−4.57 (−4.62)[c]	0.34	−4.23 (−4.28)[d]	−4.71 (−4.56)[c]	−0.04	−4.75 (−4.60)[d]	−4.70 (−5.16)[c]	2.37	−2.33 (−2.79)[d]
Δ(sum)[b]	0.00	0.00	0.00	−0.15	−0.38	−0.53 (−0.32)[e]	−0.13	2.03	1.90 (1.49)[e]

[a] To distinguish the hydrogen atoms, the symbols X,Y, Z, and W are used. The reaction is described as H + XCYZOW → XH + CYZOW. [b] Difference with respect to the values at reactants. [c] Values in parentheses are ΔG_{ENP}. [d] Values in parentheses are ΔG_S^0 calculated by eq 16. [e] Values in parentheses are computed from ΔG_S^0 rather than from $\Delta G_{EP} + G_{CDS}$.

TABLE 11: Saddle Point Structures H−X−CYZOW[a]

	AC-SRP	HF||AM1-SRP	
	SES	SES	ESP
r_{H-X}	0.971	0.867	0.854
r_{X-C}	1.323	1.277	1.278
r_{C-Y}	1.091	1.088	1.082
r_{C-Z}	1.085	1.088	1.083
r_{C-O}	1.368	1.387	1.396
r_{O-W}	0.959	0.972	0.984
θ_{HXC}	177.85	178.51	178.08
θ_{XCY}	103.36	106.41	105.99
θ_{XCZ}	103.57	106.37	105.46
θ_{XCO}	110.91	108.18	107.68
θ_{COW}	109.18	109.70	108.41
ϕ_{HXCY}	121.97	75.53	128.02
ϕ_{HXCZ}	239.83	197.10	249.12
ϕ_{HXCO}	357.58	313.33	5.73
ϕ_{HCOW}	71.53	67.78	71.26

[a] Bond distances r in Å, bond angles θ and torsion angles ϕ in degrees.

TABLE 12: Gas-Phase Reaction Rate Constants in cm^3 Molecule^{-1} s^{-1}

temp (K)	AC-SRP CVT/SCT	HF||AM1-SRP CVT/SCT	HF||AM1-SRP CVT/μOMT	expt
200	1.8 (−16)	8.0 (−16)	1.3 (−15)	
250	1.0 (−15)	2.9 (−15)	4.8 (−15)	
282	2.5 (−15)	6.0 (−15)	9.5 (−15)	
298	3.8 (−15)	8.3 (−15)	1.3 (−14)	2.8 (−15)[a]
300	4.0 (−15)	8.7 (−15)	1.3 (−14)	3.1 (−15)[a]
325	7.0 (−15)	1.4 (−14)	2.1 (−14)	6.0 (−15)[a]
359.4	1.4 (−14)	2.5 (−14)	3.5 (−14)	1.3 (−14)[a]
400	2.8 (−14)	4.5 (−14)	6.1 (−14)	2.8 (−14)[a]
500	1.0 (−13)	1.5 (−13)	1.8 (−13)	1.3 (−13)[b]
600	2.8 (−13)	3.6 (−13)	4.2 (−13)	4.3 (−13)[b]
1000	2.9 (−12)	3.3 (−12)	3.4 (−12)	6.5 (−12)[b]
1500	1.3 (−11)	1.4 (−11)	1.4 (−11)	3.5 (−11)[b]
2000	3.4 (−11)	3.4 (−11)	3.4 (−11)	9.5 (−11)[b]
2400	5.8 (−11)	5.6 (−11)	5.7 (−11)	

[a] From Aders (ref 69). [b] From Tsang (ref 23).

2.6. Software. For AC-SRP, all electronic structure calculations were carried out with the Gaussian94[58] program combined with the mn-gsm98.2.3[59] solvation module. Gas-phase and solution dynamics calculations for AC-SRP were carried out with a prerelease version of gaussrate8.1,[60] based on polyrate8.1[61] and Gaussian94.[58] The HF||AM1-SRP calculations were carried out with the gamess[62] program (version of May 1998) with the gamesol2.1[63] solvation module. Dynamics calculations at the HF||AM1-SRP level were carried out using a prerelease version of gamesolrate8.1,[64] based on polyrate8.1[61] and gamesol2.1.[63]
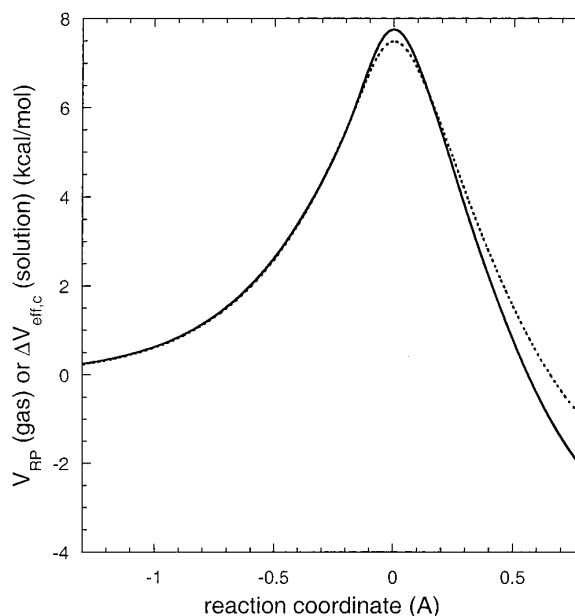
Figure 2. Born−Oppenheimer energy $V_{RP}(s)$ along the gas-phase reaction path (solid curve) compared to the aqueous potential of mean force along the gas-phase (dashed curve) reaction path; both curves are calculated by AC-SRP. Note that $\Delta V_{eff,c}(s) \equiv V_{eff,c}(s) - V_{eff,c}(s = -\infty)$, where $V_{eff,c}(s)$ is defined in eq 7.

3. Experimental Situation

3.1. All-Protium Reaction. There are three reactive channels for hydrogen atom abstraction from a methanol molecule by a hydrogen atom, the formation of $H_2 + CH_2OH$ (channel 1), of $H_2 + CH_3O$ (channel 2), and of $H_2O + CH_3$ (channel 3). Lendvay et al.[20] calculated the reaction barrier heights of these reactions using ab initio methods and showed that channel 3 has a much higher barrier than the other two. Furthermore, they showed that channel 2 also has a much higher barrier than channel 1 such that it contributes only 4% at 1000 K and less than 0.1% at room temperature. Their calculations supersede earlier, less reliable estimates of the rate of channel 2, which led to a recommendation that the measured rate constant might contain as much as a 20% contribution from channel 2. Therefore, unlike previous workers, we do not make any correction to the measured rate constants to subtract out channel 2 in either the gas phase or the liquid solution phase.

Comparison to experiment must take account of experimental errors. To eliminate fluctuations of individual data points and

Direct Dynamics for Free Radical Kinetics in Solution

J. Phys. Chem. A, Vol. 103, No. 25, 1999 **4901**

to provide a consistent comparison of gas-phase and liquid data at a single temperature, all experimental values are evaluated at 298.0 K from linear Arrhenius fits provided by the experimetalists in their original publications or from the nonlinear Arrhenius fit of Tsang[23] in his review article.

Consider first the liquid-phase data in aqueous solution. The Arrhenius fit of Mezyk and Bartels[6] agrees with previous work[65,66] within about 25% for 288−295 K but differs from previous measurements by a factor of 1.7 (lower than previous work by Smaller et al.[65]) at 281 K and a factor of 1.8 (higher than previous work by Neta et al.[66]) at 303 K.[6] However, the EPR method used in ref 6 is expected to be much more accurate than the methods applied previously, and the rate of reaction 1 was measured quite often to serve as a standard; therefore, the uncertainty is expected to be no greater than a factor of 1.5.[67] We therefore estimate an uncertainty of a factor of 1.5 in the value we obtain from the fit of ref 6, which is $k_{aq} = 5.0 \times 10^{-15}$ cm^3 molecule^{-1} s^{-1} at 298 K.

In the gas phase, Tsang[23] provided a recommendation over the range 500−2000 K. There are no data available above 2000 K, and he does not have a recommendation below 500 K because of uncertainties in the data.[68] Tsang estimates a factor of 3 uncertainty at 2000 K and a factor of 1.5 uncertainty at 500 K. The only measurements that extend below 500 K are those of Aders[69] and Meagher et al.[70] The averaged measured value of Meagher et al. leads to 3.9×10^{-15} cm^3 molecule^{-1} s^{-1} at 298 K. However, they consider that their directly measured value is probably unreliable due to mechanistic complications and suggest combining their measured activation energy with a preexponential factor equal to one-half their measured preexponential factor for H + CH$_3$OCH$_3$ (because there are only half as many abstractable hydrogens). This would decrease the rate constant to 1.1×10^{-15} cm^3 molecule^{-1} s^{-1} at 298 K. Although this correction factor was accepted by Tsang (who misquoted the temperature range of Meagher et al.[70] as 300−404 K rather than 298−575 K), we believe it is very dangerous because CH$_3$OH and CH$_3$OCH$_3$ have different barrier heights and barrier widths and hence different amounts of tunneling, and this could lead to significantly different curvatures of their Arrhenius plots. Furthermore, this theoretical correction of their measured rate constant makes it agree much less well with the result of Aders,[69] which is 2.8×10^{-15} cm^3 molecule^{-1} s^{-1} at 298 K. In light of these uncertainties in the results of Meagher et al., we will use the results of Aders as the best estimates of the experimental rate constants below 500 K. However, we estimate an uncertainty of at least a factor of 3 in this value.

The ratio k_{aq}/k_{gas} is thus estimated to be about 1.8 at 298 K, with an experimental uncertainty estimated to be at least a factor of 3. The present best estimate of the experimental value of the aqueous acceleration is larger than the experimental estimate used by Mezyk and Bartels[6] (80% vs 23%), but it agrees with it within the experimental uncertainty.

3.2. Deuterium Attack Reaction. Meagher et al.[70] also measured the deuterium attack reaction, i.e., •D + CH$_3$OH, in the gas phase. They found k_{DH} (where the first subscript denotes the attacking atom and the second denotes the transferred atom) to be 6.9×10^{-15} cm^3 molecule^{-1} s^{-1} at 298 K. This leads to a value of 0.56 for the k_{HH}/k_{DH} kinetic isotope effect (KIE). Although the absolute reaction rate of the hydrogen transfer reaction in Meagher's experiment is not, in our opinion, as reliable as the values from Aders' experiment, Meagher's experiement provides the best available experimental information on the gas-phase KIE (under the assumption that the errors
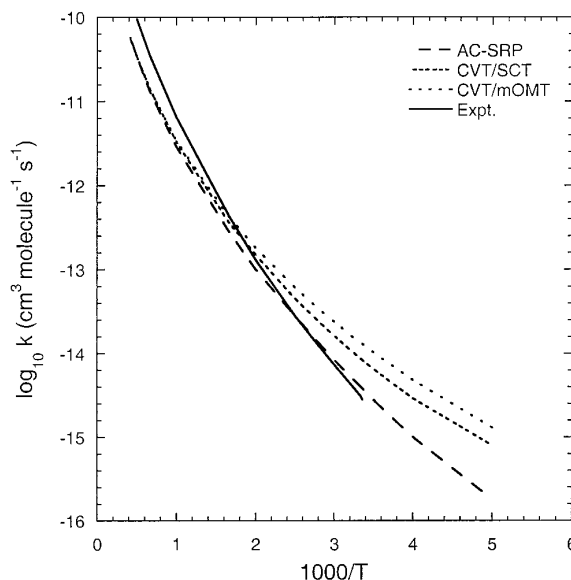
Figure 3. Arrhenius plot of calculated and exprimental gas-phase rate constants for reaction 1.

approximately cancel in the KIE), and thus we accept their value for the gas-phase KIE. Lossack et al.[71] measured the D + CH$_3$OD reaction in aqueous solution and obtained a value of $k_{HH}/k_{DH} = 0.71$ for the aqueous KIE. (Note that in the gas-phase experiment the W atom in H + XCYZZOW is H, whereas in the aqueous experiment the W is D.) We carried out a full dynamics calculation for the reaction D + CH$_3$OD both in solution and in the gas phase.

3.3. Deuterium Transfer Reaction. The gas-phase rate constant for the H + CD$_3$OH → HD + CD$_2$OH reaction is not known, but the reaction rate has been measured in aqueous solution by Anbar et al.,[72] and they estimated 20 for the kinetic isotope effect k_{HH}/k_{HD}.

4. Discussion

In comparing the theoretical results to experiment, the reader should keep in mind that absolute reaction rates are very sensitive to small changes in barrier heights, which are uncertain. Thus, we can learn more about the physical effects responsible for solvent effects on reaction rates from ratios of rate constants than from absolute rate constants.

We note that conventional TST, CVT, and CVT/SCT may be considered to be successively more complete theories. We do not present all these levels as competing theories but rather as approximations to our most complete dynamical level, CVT/μOMT; it is interesting to study the lower level dynamical results because examination of the less complete dynamical calculations helps us to understand how important it is to include the higher level dynamical effects. The same spirit applies to the comparisons of SES results to ESP results; SES theory is an approximation to the more complete ESP theory.

4.1. All-Protium Reaction. *4.1.1. Gas Phase.* An Arrhenius plot of the gas-phase rate constants is given in Figure 3, and it shows nonlinearity at lower temperatures, which is primarily due to the large amount of tunneling at these temperatures. The nonlinearity is reflected in different values for the gas-phase activation energy as a function of the temperature range over which the slope is measured or calculated. With the AC-SRP method, the activation energy obtained from the local slope of

4902 *J. Phys. Chem. A, Vol. 103, No. 25, 1999*

Chuang et al.

TABLE 13: Rate Constants[a] of Reaction 1 at 298 K and Ratios of Liquid-Phase Rate Constants to Gas-Phase Ones

source	method	k(gas)	k(liquid) SES	ESP	k(liquid)/k(gas) SES	ESP
experimental		2.8[b]		5.0[c]		1.8[b]
AC-SRP	TST[d]	0.6	0.9		1.6	
	CVT	0.5	0.8		1.5	
	CVT/ZCT	1.3	1.6		1.2	
	CVT/SCT	3.8	3.8		1.0	
HF||AM1-SRP	TST[d]	1.1	1.7	2.2	1.5	2.0
	CVT	0.7	0.9	1.9	1.2	2.7
	CVT/ZCT	2.0	2.4	4.8	1.2	2.4
	CVT/SCT	8.3	8.7	16.6	1.1	2.0
	CVT/LCT	12.7	12.5	25.7	1.0	2.0
	CVT/μOMT	12.9	12.7	25.9	1.0	2.0

[a] k in units of 10^{-15} cm^3 molecule^{-1} s^{-1}. [b] Uncertainty: at least a factor of 3 (see text). [c] Uncertainty: factor of 1.5 (see text). [d] TST denotes conventional transition state theory; that is, the free energy of activation is evaluated at the saddle point, and tunneling is neglected.

the Arrhenius plot is 5.66 kcal/mol for the range 300−600 K, while the activation energy obtained for the range 600−1000 K is 7.08 kcal/mol.
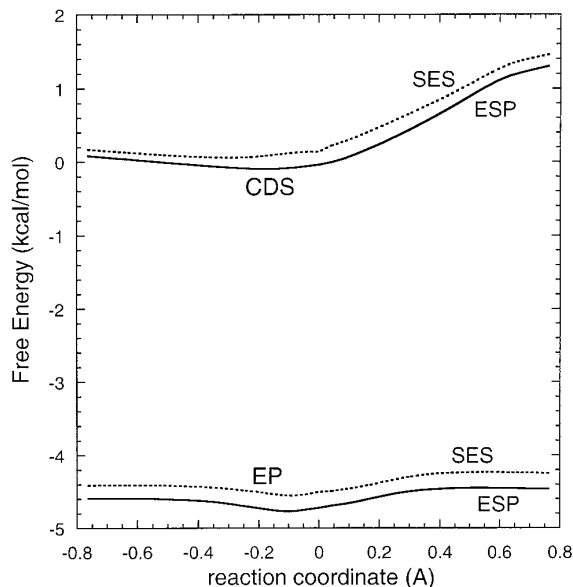
Table 12 shows that we obtain good agreement with gas-phase experiments over the entire temperature range if we take account of the experimental uncertainties (factor of 3 at the extremes of the experimental temperature range but about 1.5 near 500 K). In fact, we agree with experiment within the experimental uncertainty (although our slope is somewhat smaller). Of course, this agreement is partly by construction since the AC-SRP parameters were adjusted in part to give a reasonable barrier height. This confirms that the adjustment does yield a reasonable solventless (i.e., gas-phase) barrier height. Based on comparing the magnitudes of the rate constants and the temperature dependencies of the theoretical and experimental results in Table 12, we conclude that the theoretical barrier heights of the potential energy surfaces used in this paper may be too low by about 1.2 ± 1 kcal/mol; that is, the best estimate of the true barrier height is probably 9 ± 1 kcal/mol. In light of the uncertainties in the experiments, further adjustment of the semiempirical parameters in our potential surfaces was not pursued.

4.1.2. Liquid Phase. Our main focus is on solvent effects, to which we turn next. The solution-phase rate constants at 298 K are shown in Table 13. The SES/AC-SRP/CVT/SCT rate constant at 298 K is 3.8 × 10^{-15} cm^3 molecule^{-1} s^{-1}, which agrees well with experiment. The HF\|\|AM1-SRP method results in an SES/CVT/SCT rate constant that is 2.3 times higher than that from AC-SRP and 1.7 times higher than experiment, still within our assigned experimental error bar. For the HF\|\|AM1-SRP potential surface, we also carried out the tunneling calculation by the more reliable μOMT method, which increases the calculated rate constant by another factor of 1.5, making it 2.5 times bigger than experiment. At the SES level, the ratio of k(liquid) to k(gas) is reasonably consistent between the AC-SRP and HF\|\|AM1-SRP energy surfaces, and it decreases as the dynamical level is increased, from 1.5−1.6 at the conventional TST dynamical level to 1.0−1.1 when variational effects and tunneling are included. The fact that these ratios are similar for the quite different AC-SRP and HF\|\|AM1-SRP approaches is very encouraging. It is not 100% clear what to make of the final value of k(liquid)/k(gas) = 1.0 in the separable equilibrium solvation calculation. On one hand, this does fall within the experimental error bars, and it is reasonably close to Mezyk and Bartels' analysis showing only a 23% acceleration (i.e., k(liquid)/k(gas) ≈ 1.2), but on the other hand, our own analysis
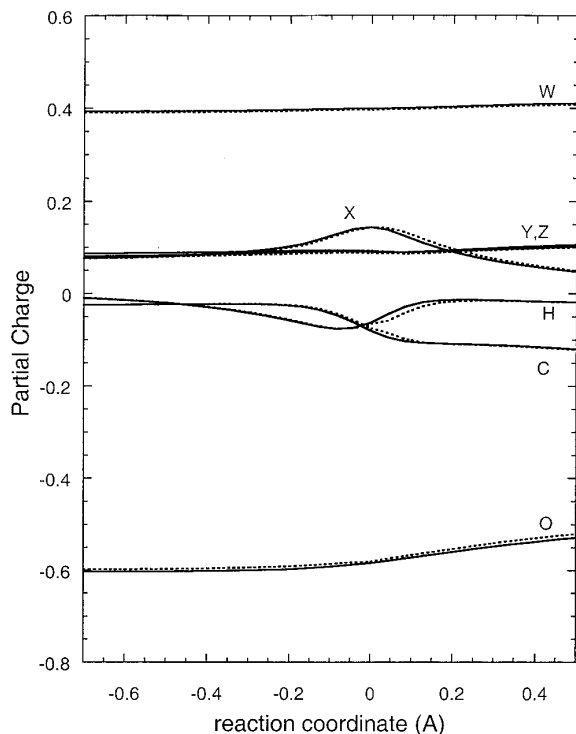
of experiment and our identification of the *best* experimental values indicates an 80% acceleration of the reaction rate by the solvent in water (i.e., k(liquid)/k(gas) ≈ 1.8). Nevertheless, it is very instructive to examine the various factors contributing to k(liquid)/k(gas) in the SES approximation, especially since the final value of ∼1.0 results from a cancellation of solvent effects rather than an absence of solvent effects. For example, Table 8 shows a large change in the electronic polarization free energy of the oxygen atom as we move from the reactants to the saddle point; ΔG_{EP} of this atom becomes less negative. At the same time, the ΔG_{EP} values of the alcoholic hydrogen atom and one of the hydrogens from the methyl group become more negative, and the net result is to make ΔG_{EP} more negative by 0.3 kcal/mol, thereby accelerating the reaction in aqueous solution by a factor of 1.7. There is no discernible hydrophobic acceleration, and the cavity dispersion solvent structure term does not change much, although it does lower the final value of k(liquid)/k(gas) as calculated by conventional transition state theory (see Table 13) to 1.6.

As we move toward the product side, the overall ΔG_{EP} becomes 0.2 kcal/mol less negative than that for reactants, and it becomes 0.5 kcal/mol less negative than the value at the saddle point. As we move to the products, G_{CDS} increases about 1.8 kcal/mol and results in a total increase of 1.98 kcal/mol in the free energy of solvation ΔG_S^0. (The values just mentioned are for AC-SRP, but comparison of Table 9 to Table 8 shows that HF\|\|AM1-SRP provides a similar picture.) The fact that the free energy of aqueous solvation decreases the free energy profile by ∼0.3 kcal/mol at the saddle point but increases it by ∼2.0 kcal/mol at the product causes the true dynamical bottleneck to be later than the saddle point; this is an example of a "parallel effect" in the language[73] of Albery−More O'Ferrall−Jencks diagrams. This displacement of the dynamical bottleneck toward products is barely visible in Figure 2, but it decreases the aqueous acceleration factor from 1.6 to 1.5. The effect is larger, 20% instead of 6% in the HF\|\|AM1-SRP calculations, reducing k(liquid)/k(gas) from 1.5 at the TST level to 1.2 at the CVT level. Then, when we include the quantum mechanical tunneling effects in the dynamics calculation by the SCT approximation, the reaction rate in solution does not increase as much as the gas-phase one, and the final liquid-phase rate constant differs from the gas-phase value by only 1−2% at 298 K for either energy surface.

To explore further the factors contributing to the possibility that the aqueous rate is significantly accelerated relative to the gas-phase rate, we carried out an ESP calculation with the HF\|\|AM1-SRP method. In the ESP calculation, the geometries of the stationary points are optimized using an effective potential that is a sum of the gas-phase potential and the free energy of solvation. Table 10 shows that solvation effects are more favorable at the transition state in this more complete calculation, both due to electronic electric polarization terms and due to CDS terms. Figure 4 shows the G_{CDS} and G_P along the reaction path for the HF\|\|AM1-SRP method with SES and ESP approximations. The values of the SES calculation (dotted curves) are consistently higher than the values in the ESP approximation (solid curves) by about 0.2 kcal/mol. Figure 5 shows the partial charges of the atoms along the reaction path with SES and ESP approximations. The difference between the SES and ESP values of G_{CDS} is due almost entirely to the oxygen atom. The hydrogen atom of the hydroxyl group has the most positive charge and the oxygen atom of the hydroxyl group has the most negative charge, and these two atoms contribute almost all the difference between the SES and ESP values of G_{EP}. The charge of the

Direct Dynamics for Free Radical Kinetics in Solution
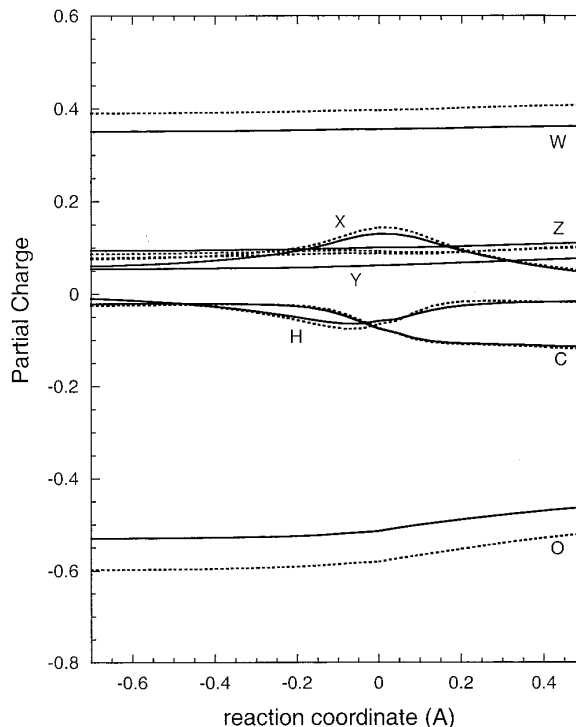
J. Phys. Chem. A, Vol. 103, No. 25, 1999 **4903**

Figure 4. Free energies of the electric polarization contribution (G_{EP}) and the cavitational dispersion structural contribution (G_{CDS}) along the reaction path of the HF||AM1-SRP method with SES (in dotted curves) and ESP (in solid curves) approximations.
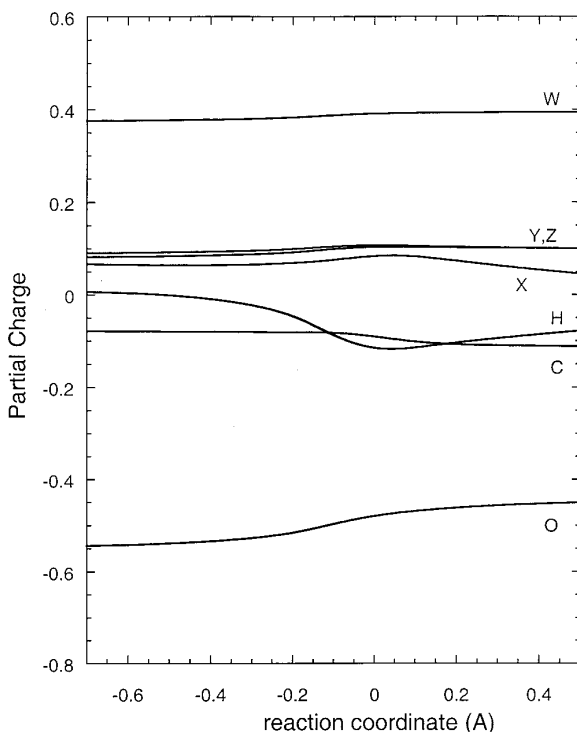

Figure 6. HF||AM1-SRP partial atomic charges in atomic units along the gas-phase reaction path; solid curves are for the gas phase, and dotted curves are aqueous results in the SES approximation.

present already in the gas phase, although the magnitudes of most charges are increased by dielectric screening in the liquid. Finally, Figure 7 presents the liquid-phase SES charges from the AC-SRP calculations. Comparison of these charges to the SES charges in either Figure 5 or 6 shows encouraging agreement for the trends in the *s* dependencies, with the biggest difference being the smaller variation in q_X in the AC-SRP calculation.

The rate constants from the gas-phase calculations are given in Table 12, and the aqueous reaction rate constants are given in Table 13. Furthermore, the solvation effect increases from 2.0 to 2.7 when the maximum free energy of activation is found. This is high enough so that the ratio remains above the "best" experimental estimate of 1.8 even after tunneling reduces it 26% from 2.7 to 2.0.

Because tunneling plays a significant role in the solvation effect, it is interesting to examine it in more detail. For this reason, we have included an intermediate level of tunneling calculation in Table 13, namely zero curvature tunneling (ZCT). In ZCT tunneling, $V_{eff,c}(s)$ is the same as for SCT tunneling, but reaction path curvature is not included in the effective reduced mass. Thus, the solvation effect on tunneling arises entirely from the shape of $V_{eff,c}(s)$ in the ZCT approximation. Table 13 shows that, in the AC-SRP calculations, 60% of the tunneling reduction in k(liquid)/k(gas) occurs already at the ZCT level. The broadening of the effective barrier that accounts for this is readily apparent in Figure 2. However, in the HF||AM1-SRP calculations, the tunneling reduction comes not from the change in shape of the effective barrier along the classical reaction path (as would show up in the ZCT calculation) but rather from the deviations of the average tunneling path from the classical reaction path (as show up in $\mu_{eff}(s)$ or in the LCT calculations). These deviations, which could be zero in the

Figure 5. Partial atomic charges in atomic units along the reaction path of the HF||AM1-SRP method in SES (in dotted curves) and ESP (in solid curves) approximations. In Figures 5−11, we use the labeling scheme: H + XCYZOW → HX + CYZOW.

carbon atom becomes slightly negatively charged toward the product region due to the formation of the radical. Figure 6 compares the gas-phase and liquid-phase charges along the gas-phase reaction path. This figure shows that the basic trends observed in Figure 5 (in particular the nonmonotonic behavior of q_H and q_X, the decrease of q_C, and the increase of q_O), are

4904 *J. Phys. Chem. A, Vol. 103, No. 25, 1999*

Chuang et al.

Figure 7. AC-SRP partial atomic charges in atomic units along the gas-phase reaction path as computed by the SES approximation for aqueous solution.

absence of reaction path curvature in the barrier region, increase the tunneling probability, and the calculations in Table 13 show that they are more significant in the gas phase than in solution. For the AC-SRP calculations, this appears to result primarily from the fact that reaction path curvature effects amplify any differences that are already apparent at the ZCT level, whereas in the HF||AM1-SRP calculation the effect appears more subtle and is apparently due to a solvation-induced shift in the alignment of region of highest curvature with the barrier top.

One should also note that, even in the gas phase, the ESP/CVT/SCT reaction rates calculated by HF||AM1-SRP are a factor of 2.2 higher than those calculated by AC-SRP. This increase is a product of these factors: a factor of 1.34 at the CVT level (the barrier height effect), a 1.15-fold increase due to ZCT tunneling (the barrier width effect), and a final factor of 1.44 due to reaction path curvature. For the HF||AM1-SRP energy surface, we were also able to show that large-curvature tunneling results in a further increase of another factor of 1.55. This latter factor is perhaps surprising since large-curvature tunneling is often associated with the heavy−light−heavy mass contribution rather that the present light−light−heavy (H−H−CH$_3$OH) mass combination.[74] Nevertheless, large-curvature tunneling effects of this size are also known for other light−light−heavy cases, e.g., $k^{\mu OMT}/k^{SCT}|_{300K} = 1.35$ for H−H−O and 1.46 for H−H−Cl.[75]

We also note that the HF||AM1-SRP reaction rates estimated by CVT/SCT and CVT/μOMT are higher than the experimental results by more than the estimated experimental error bar. We believe though that at the present state of knowledge, one should not pay as much attention to absolute reaction rate constants as to rate constant ratios. Thus, for example, the fact that LCT tunneling increases the rate constants is physically significant; the fact that it takes the calculated value farther from the best

experimental estimate is just an artifact of the theoretical barrier height apparently being slightly too low. The comparisons of absolute reaction rates are hampered by uncertainties in the experiments, uncertainties in the absolute barrier height, and uncertainties about nonequilibrium effects. But the rate constant ratios still help us to ascertain the *factors* which must eventually be understood and converged if we are to ultimately make our theoretical treatments of this kind of reaction reliable. With this motivation, we next discuss two more kinds of ratios: (i) k^{ESP}/k^{SES} and (ii) kinetic isotope effects.

As noted above, the SES calculations, although identifying some factors that accelerate the reaction in liquid-phase solution, do *not* predict a net speedup of the reaction rate in solution. However, in the ESP approximation, a speedup of the reaction in solution *is* observed and the calculated ratio k(liquid)/k(gas) equals 2 (where the experimental value is estimated to be 1.8, see above).

We found that the tunneling effect is quenched by solvent to a similar extent in the SES or ESP calculations. To place this in a more quantitative context, we use the HF||AM1-SRP calculations to factor the k^{ESP}/k^{SES} ratio as follows:

$$\frac{k_{ESP}^{CVT/\mu OMT}}{k_{SES}^{CVT/\mu OMT}} = \left(\frac{\kappa_{ESP}^{\mu OMT}}{\kappa_{SES}^{\mu OMT}}\right)\left(\frac{k_{ESP}^{CVT}/k_{ESP}^{TST}}{k_{SES}^{CVT}/k_{SES}^{TST}}\right)\left(\frac{k_{ESP}^{TST}/k_{GAS}^{TST}}{k_{SES}^{TST}/k_{GAS}^{TST}}\right) \quad (20)$$

where the transmission coefficient κ is the ratio of $k^{CVT/\mu OMT}$ to k^{CVT}. Thus, the values in parentheses in eq 20 indicate respectively the relative contributions from the tunneling effect, the variational effect, and conventional TST in the SES and ESP approximations. The left-hand side of eq 20 equals 2.04 in the HF||AM1-SRP calculation, and the contribution from the tunneling effect is 0.9, from variational effects is 1.72, and from the saddle point is 1.32. Therefore, in this factorization, the factor of 2 in speedup observed in the ESP approximation is mainly contributed by the variational effect, i.e., the effect on the rate constant of variationally determining the maximum of the free energy profile (see eq 13) rather than placing it at the conventional transition state at $s = 0$.

Recall that the difference in the SES and ESP approximations is that in SES we use the gas-phase reaction path and add the free energy of solvation at each point, whereas in the ESP approximation the reaction path is followed in the bath. To study the difference of the transition-state variational effect in these approximations, we had to locate the dynamical bottleneck, which is the maximum of the free energy profile at 298 K. For the SES calculation, the bottleneck is located at $s = 0.10$ Å, where the free energy (G^0 of eq 4 with the zero of V placed at reactants) equals 38.41 kcal/mol, and the free energy profile in the ESP approximation has a maximum at $s = 0.06$ Å with $G^0 = 37.92$ kcal/mol. The difference of 0.49 kcal/mol in the free energy corresponds to the factor of 2.3 that the $k_{ESP}^{CVT}/k_{SES}^{CVT}$ ratio equals at 298 K. The classical energies and the zero-point energies at the dynamical bottlenecks can be obtained by linearly interpolating between the closest two saved points on the reaction path. For the ESP approximation, the classical energy V_{RP} is 7.25 kcal/mol and the zero-point energy (ZPE) is 33.35 kcal/mol, whereas these values equal 7.00 and 33.83 kcal/mol in the SES approximation. We then partition the −0.49 kcal/mol that we obtained for $G_{ESP}^{0,CVT} - G_{SES}^{0,CVT}$ into −0.25 kcal/mol from the classical effective potential energy (which is the sum of Born−Oppenheimer energy and free energy of solvation), +0.48 kcal/mol from ZPE, and −0.34 kcal/mol from thermal vibrational−rotational energy.

Direct Dynamics for Free Radical Kinetics in Solution

J. Phys. Chem. A, Vol. 103, No. 25, 1999 **4905**

TABLE 14: Saddle Point of R1 in SES and ESP Approximations at 298 K

	AC-SRP SES	HF||AM1-SRP SES	HF||AM1-SRP ESP
V (kcal/mol)^a	7.75	7.77	
$\Delta V_{\text{eff,c}}$ (kcal/mol)^b	7.48	7.54	7.46
ΔV_{eff} (kcal/mol)^c	39.48	40.47	40.56
$R^{\ddagger}_{\text{H–H}}$ (Å)	0.971	0.841	0.854
$R^{\ddagger}_{\text{C–H}}$ (Å)	1.322	1.297	1.281
$q_{\text{O}}{}^d$	−0.480	−0.495	−0.494
$q_{\text{W}}{}^d$	0.391	0.365	0.366
$q_{\text{X}}{}^d$	0.084	0.109	0.110
$q_{\text{H}}{}^d$	−0.115	−0.059	−0.057
ν_1 (O–H str.)	3924^e	3680	3500
ν_2 (C–H str.)	3265	3412	3461
ν_3 (C–H str.)	3134	3388	3435
ν_4	1547	1786	1866
ν_5	1501	1561	1639
ν_6	1437	1474	1529
ν_7	1377	1438	1447
ν_8	1364	1387	1389
ν_9	1220	1292	1288
ν_{10}	1169	1199	1191
ν_{11}	1121	1156	1148
ν_{12}	606	574	590
ν_{13}	395	386	392
ν_{14}	326	304	279
ν_{15}	1450i	1826i	1797i

^{a} Gas-phase Born–Oppenheimer energy with respect to the energies of the reactants. ^{b} Classical effective potential energy with respect to the classical effective potential of the reactants (see eqs 7 and 17). ^{c} Effective potential energy (see eq 6) with respect to the classical effective potential of the reactants, i.e., V_{eff} ($s = 0$) − V_{eff} (s = reactants). ^{d} To distinguish the hydrogen atoms, the symbols X, Y, Z, and W are used. The reaction is described as H + XCYZOW → CYZOW + XH. ^{e} Frequencies are in cm^{-1}.

Table 14 gives the saddle-point information for the aqueous reaction calculated with AC-SRP and HF\|\|AM1-SRP at 298 K. From the vibrational frequency ν_m of mode m, we can calculate its contribution to the rate constant, which is given by the partition function Q_m with the zero of energy at the saddle point. Note that

$$Q_m = \tilde{Q}_m \, e^{-Z_m/\tilde{k}T} \qquad (21)$$

where Z_m is the zero-point energy of mode m, $\tilde{k}$ is Boltzmann's constant, and $\tilde{Q}_m$ is the usual partition function that tends to unity as $T \to 0$. From the HF\|\|AM1-SRP frequencies in Table 14, we find that $Q_m^{\text{ESP}}/Q_m^{\text{SES}}$ exceeds 1.10 for only two modes, $m = 1$ and 14, for which it equals 1.54 and 1.10, respectively. (The former value reflects a significant difference in the O–H bond distance, which is 0.99 Å in the ESP and 0.97 Å in the SES approximation, and the latter reflects an increase in both the C–O and O–H bond lengths.) However, $Q_m^{\text{ESP}}/Q_m^{\text{SES}}$ is in the range 0.82–0.89 for all of modes $m = 2$–6, and the accumulation of these small effects dominates the product of all $Q_m^{\text{ESP}}/Q_m^{\text{SES}}$ ratios; the product is 0.78. This vibrational contribution to $k^{\text{ESP}}/k^{\text{SES}}$ from the saddle point is, in turn, dominated by a factor of 0.68 from reactants, due primarily to a factor of 0.62 from $m = 5$ and 0.82 from $m = 9$, partly canceled by factors of 1.22 from $m = 1$ and 1.21 from $m = 12$. Putting the reactant and transition state contributions together, the vibrational contribution to the rate constant is then 1.14 (=0.78/0.68), which consists of 1.26 from $m = 1$, 0.75 from $m = 2$–6, and 1.19 from the rest. In perspective, the vibrational contribution of a factor of 1.14 to $k^{\text{ESP}}/k^{\text{SES}}$ accounts for 44% of the effect of optimizing geometries and reaction paths in

TABLE 15. CVT Reaction Bottleneck of R1 in SES and ESP Approximations at 298 K

	AC-SRP SES	HF||AM1-SRP SES	HF||AM1-SRP ESP
s (bohr)	0.0609	0.1837	0.1129
$\Delta V_{\text{eff,c}}$ (kcal/mol)^a	7.42	7.01	7.10
ΔV_{eff} (kcal/mol)^b	39.53	40.86	40.63
$R^{\text{CVT}}_{\text{H–H}}$ (Å)	0.94	0.79	0.79
$R^{\text{CVT}}_{\text{C–H}}$ (Å)	1.36	1.35	1.34
$q_{\text{O}}{}^c$	−0.476	−0.533	−0.541
$q_{\text{W}}{}^c$	0.392	0.403	0.404
$q_{\text{X}}{}^c$	0.083	0.109	0.112
ν_1 (cm^{-1})	3923	3660	3503
ν_2 (cm^{-1})	3270	3464	3481
ν_3 (cm^{-1})	3138	3447	3451
ν_4 (cm^{-1})	1632	2525	2420
ν_5 (cm^{-1})	1546	1572	1601
ν_6 (cm^{-1})	1432	1475	1505
ν_7 (cm^{-1})	1351	1443	1436
ν_8 (cm^{-1})	1347	1314	1316
ν_9 (cm^{-1})	1222	1199	1201
ν_{10} (cm^{-1})	1154	1141	1140
ν_{11} (cm^{-1})	1118	1106	1109
ν_{12} (cm^{-1})	611	617	616
ν_{13} (cm^{-1})	396	393	393
ν_{14} (cm^{-1})	322	317	283

^{a} Classical effective potential energy with respect to the classical effective potential of the reactants (see eqs 7 and 17). ^{b} Effective potential energy (see eq 6) with respect to the classical effective potential of the reactants, i.e., V_{eff} ($s = 0$) − V_{eff} (s = reactants). ^{c} To distinguish the hydrogen atoms, the symbols X, Y, Z, and W are used. The reaction is described as H + XCYZOW → CYZOW + XH.

solution at the conventional TST level since $k^{\text{ESP}}/k^{\text{SES}} = 1.32$ at the conventional TST level (see Table 13). This in turn is 32% of the final $k^{\text{ESP}}/k^{\text{SES}}$ value of 2.0, which results primarily from a large increase in this ratio at the CVT level, which is partly canceled by the tunneling effect (again see Table 12). The main lesson to be learned from this dissection is that the final overall solvent effect results from many, many contributions in both directions, which partly cancel. (This is an important result in that it shows by example why very simple explanations, although appealing, cannot be trusted.) Nevertheless, the above discussion shows that a large part of the enhancement of k(liquid) over k(gas) comes from variational transition state effects and vibrations.

Table 15 gives information about the aqueous CVT reaction bottlenecks calculated with AC-SRP and HF\|\|AM1-SRP at 298 K. We compare the classical effective potential, the adiabatic ground-state energy, the breaking C–H bond distance, the forming H–H bond distance, and the partial charges of O and H atoms for AC-SRP and HF\|\|AM1-SRP calculations. For the HF\|\|AM1-SRP energy surface, the SES and ESP approximations lead to similar reaction bottlenecks at 298K, except that the classical effective potential differs by 0.09 kcal/mol. The AC-SRP energy surface shows an earlier bottleneck than the ones obtained by the HF\|\|AM1-SRP method.

At this point we can return to Table 10 and ask how much the hydrophobic effect contributes to k(liquid)/k(gas). We define the hydrophobic acceleration as the contribution to k(liquid)/k(gas) from the CDS terms on atoms H, X, C, Y, and Z. Table 10 shows that the sum of these CDS terms decreases by 0.52 kcal in proceeding to the conventional transition state. This effect alone would yield a solvent-induced increase in the rate constant of 2.4, which is larger than the calculated speedup of 1.32 at the TST level and is even larger than the final calculated speedup of a factor of 2.0. Thus, from this point of view, it is correct to say that the rate acceleration occurs by hydrophobic acceleration
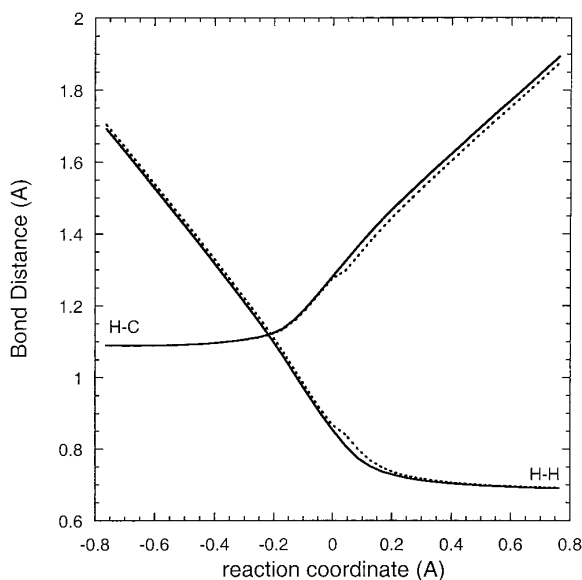
Figure 8. HF||AM1-SRP calculations of making and breaking bond distances for the aqueous reaction: (—) ESP; (- - -) SES.

partly canceled by other effects. Although it is a somewhat unsettling result, there is no way to avoid the conclusion from the discussion above that the precise amount of hydrophobic acceleration and the precise amount of cancellation result from a complicated interplay of many factors that determine the location of the dynamical bottleneck along the reaction path in the gas phase and in solution.

Six more plots illustrating the differences between the SES and ESP calculations are provided in Figures 8–13. Figure 8 shows that optimizing the reaction path in solution does not change the synchronicity of the reaction. Figures 9–11 show that the electrostatics are more sensitive than the first solvation shell effects to optimizing the reaction path in solution, and they also show which atomic sites' contributions vary strongly along the reaction path. Figures 12 and 13 illustrate the quantitative variations in the computed barrier along the reaction path. These variations will be important in the discussion that follows.

4.2. Kinetic Isotope Effects. As mentioned in the previous section, the kinetic isotope effects (KIEs) have also been studied experimentally. Table 16 shows the calculated and experimental values of the gas-phase KIEs, where k_{VX} is used to indicate $k(V + CX_3OW \rightarrow VX + CX_2OW)$; that is, the first subscript is used for the attacking species and the second subscript is used for the transfer species. Note that for k_{DH} our AC-SRP calculations are for W = D whereas the experiment is for W = H, but this does not effect our conclusions because the secondary KIE at W is very small. (We checked this with AC-SRP at the conventional TST level where we found a gas-phase ratio $k_{DH}(W = H)/k_{DH}(W = D) = 1.02$.) Meagher et al.[70] measured k_{HH}/k_{DH} (W = H) in the gas phase and obtained a value of 0.56, which may be compared to our values of 0.95 for AC-SRP/CVT/SCT, 0.82 for HF||AM1-SRP/CVT/SCT, and 0.68 for HF||AM1-SRP/CVT/μOMT. This comparison indicates that the HF||AM1-SRP energy surface may be more realistic than the AC-SRP one and also that large-curvature tunneling effects are important to get the KIE correct.

The kinetic isotope effects in aqueous solution are given in Table 17. In this case, there are two experiments: Lossack et al.[71] found 0.70 for k_{DH} (W = D); Anbar et al.[72] found 20.0 for
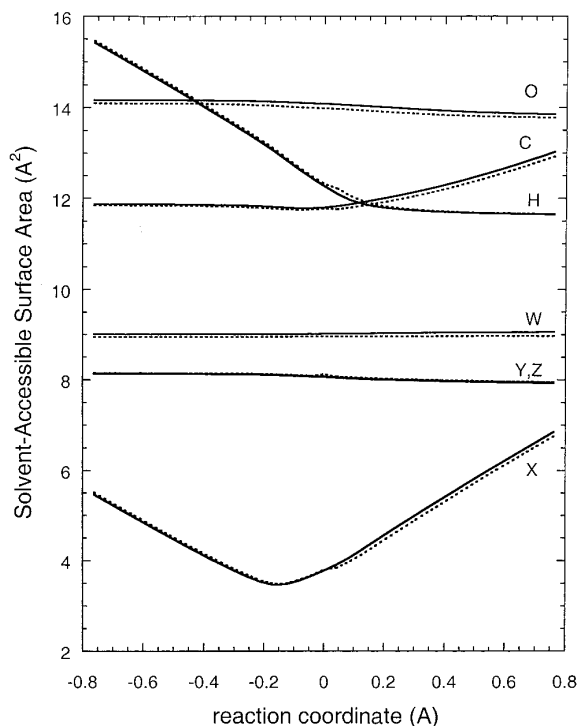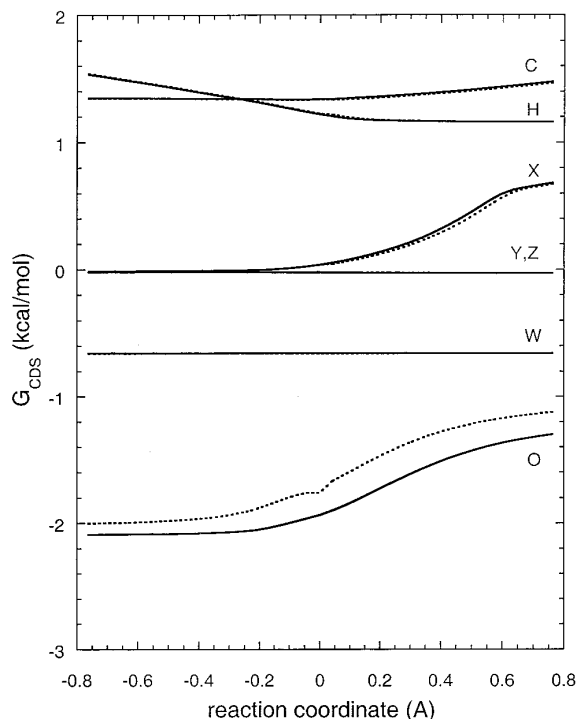

Figure 9. HF||AM1-SRP calculations of solvent-accessible surface areas of the individual atoms for the aqueous reaction: (—) ESP; (- - -) SES. In the solvation models used in this paper, the solvent-accessible surface area is the same as the exposed area of the van der Waals surface.
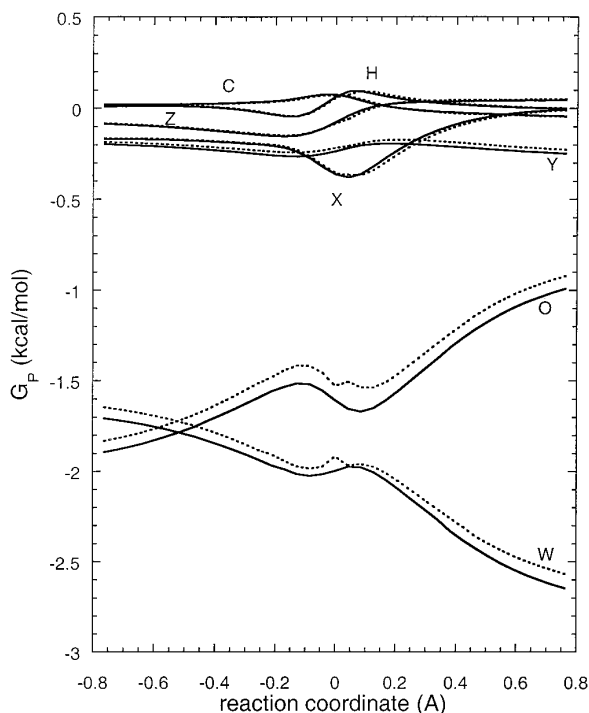

Figure 10. HF||AM1-SRP calculations of electric polarization free energy in aqueous reaction: (—) ESP; (- - -) SES.

k_{HD}. Calculations using AC-SRP and HF||AM1-SRP generated close agreement with these experimental values.

Direct Dynamics for Free Radical Kinetics in Solution

J. Phys. Chem. A, Vol. 103, No. 25, 1999 **4907**

Figure 11. HF||AM1-SRP calculations of the cavity dispersion solvent structure free energy in aqueous solution: (—) ESP; (- - -) SES.
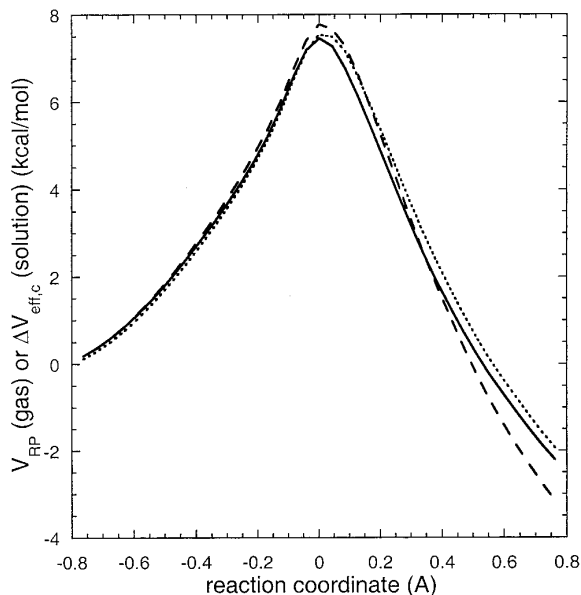
Figure 12. Born−Oppenheimer energy $V_{RP}(s)$ along the gas-phase reaction path (dashed curve) compared to the aqueous potential of mean force along the gas-phase (dotted curve) reaction path as calculated by HF||AM1-SRP and the solution-phase reaction path calculated by HF||AM1-SRP (solid curve). Note that $\Delta V_{eff,c}(s) \equiv V_{eff,c}(s) - V_{eff,c}(s = -\infty)$, where $V_{eff,c}(s)$ is defined in eq 7.

5. Summary and Conclusions

In this paper, we have introduced several new ideas for modeling implicit potential energy surfaces and potentials of mean force for direct dynamics calculations. These include the Becke three-parameter HF-DFT method with specific reaction
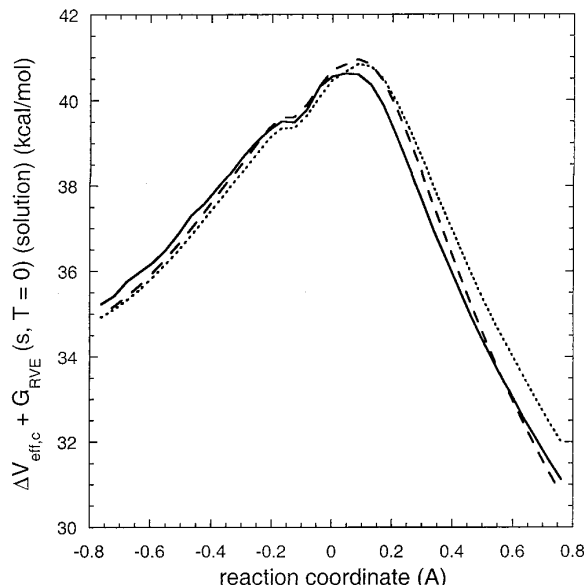
Figure 13. HF||AM1-SRP calculations of $\Delta V_{eff,c}(s) + G_{RVE}$ ($s, T = 0$): (—) ESP; (- - -) SES; (− − −) gas.

TABLE 16: Gas-Phase Kinetic Isotope Effect at 298 K

		k_{HH}/k_{DH}[a]	k_{HH}/k_{HD}[b]
experiment		0.6	
AC-SRP	TST	0.46	7.1
	CVT	0.44	7.6
	CVT/ZCT	0.63	8.2
	CVT/SCT	0.95	12.0
HF||AM1-SRP	TST	0.44	10.2
	CVT	0.29	10.6
	CVT/ZCT	0.55	9.8
	CVT/SCT	0.82	13.8
	CVT/LCT	0.67	28.0
	CVT/μOMT	0.68	21.1

[a] Theory, $k(H + CH_3OH)/k(D + CH_3OD)$; experiment, $k(H + CH_3OH)/k(D + CH_3OH)$. [b] $k(H + CH_3OH)/k(H + CD_3OH)$.

TABLE 17: Kinetic Isotope Effects at 298 K in Aqueous Solution

source	method	k_{HH}/k_{DH}[a] (W = D)		k_{HH}/k_{HD}[b]	
		SES	ESP	SES	ESP
experiment		0.7	0.7	20	20
AC-SRP	TST	0.48		7.7	
	CVT	0.44		7.8	
	CVT/ZCT	0.59		7.8	
	CVT/SCT	0.84		10.9	
HF||AM1-SRP	TST	0.44	0.39	10.3	10.3
	CVT	0.27	0.34	10.9	10.7
	CVT/ZCT	0.53	0.60	10.3	9.5
	CVT/SCT	0.81	0.91	14.6	13.3
	CVT/LCT	0.53	0.51	28.3	26.6
	CVT/μOMT	0.48	0.51	21.3	20.2

[a] $k(H + CH_3OH)/k(D + CH_3OD)$. [b] $k(H + CH_3OH)/k(H + CD_3OH)$.

parameters (denoted AC-SRP to indication its rationalization by the adiabatic connection theorem), charge model 2 with specific reaction parameters, and the linear mixing specific reaction parameter (LM-SRP) method, in particular HF||AM1-SRP, in which two energy components are mixed with an empirical coefficient. The AC-SRP approach mixes energy functionals at the level of the Fock operator for a self-consistent field or self-consistent reaction field calculation, whereas the LM-SRP approach mixes energy components at the level of

total energies in the gas-phase or potentials of mean force in solution.

Using these new methods, this paper presents one of the first attempts to quantitatively estimate the solvent effect on the rate constant of a free radical reaction in solution. Solvent effects are predicted to be much smaller than for ionic reactions, as expected. Using the AC-SRP method with parameters adjusted to gas-phase data, we carried out separable equilibrium solvation (SES) rate constants in aqueous solution, and we obtained an absolute reaction rate in aqueous solution that is within the experimental uncertainty, but we did not find a speedup of the reaction due to the solvent. The SES calculations with the AC-SRP energy surface are based on canonical variational theory (CVT) with the small-curvature tunneling (SCT) approximation.

To perform calculations with higher levels of dynamics, namely (i) equilibrium solvation path (ESP) instead of SES and (ii) microcanonical optimized multidimensional tunneling (μOMT) instead of SCT, we created a less expensive and less complicated energy surface by the LM-SRP methods; in particular, we used the HF||AM1-SRP combination. This was accomplished by a bootstrap process in which HF||AM1-SRP was optimized to AC-SRP saddle-point predictions, whose validity rests in part on the earlier parametrization of AC-SRP to experiment (this is an important point because without the AC-SRP calculation one would have less confidence in the reasonableness of the HF||AM1-SRP saddle-point geometry, and we have recently shown[56] how critical it is to employ an accurate saddle-point geometry). The ESP calculations at the CVT/μOMT level with the HF||AM1-SRP energy surface show that it is indeed important to include large-curvature tunneling in this reaction, and they yield much higher reaction rates with a solvent-induced speedup of a factor of 2, in excellent agreement with the somewhat uncertain experimental situation (estimated experimental speedup = 1.8 ± factor of 3). If we break down the effects in dynamical terms, the most significant contributor to this enhancement is the difference between the variational and conventional transition states. A smaller, but still significant, contributor is the difference in the O−H bond distance when the reaction path is optimized in solution. If instead we break down the effects in terms of the components of the free energy of solvation, we see that a major contributor is hydrophobic acceleration due to association of the hydrophobic attacking hydrogen atom with the other reactant.

Both the SES and ESP methods employing the HF||AM1-SRP energy surface with inclusion of large-curvature tunneling effects generate good agreement with experimental kinetic isotope effects.

7. Appendix

Figures 8−13 show additional comparisons of SES and ESP reaction path quantities as calculated by the HF||AM1-SRP method. Comparison of Figures 9 and 11 shows that the changes in the CDS contributions to the free energy of solvation follow more from changes in atomic surface tensions than from changes in exposed areas.

References and Notes

(1) (a) Jorgensen, W. L.; Blake, J. F.; Madura, J. D.; Wierschke, S. D. *ACS Symp. Ser.* **1987**, *353*, 200. (b) Warshel, A. *Computer Modeling of Reactions in Enzymes and in Solutions*; Wiley: New York, 1991. (c) *Advances in Physical Organic Chemistry*; Bethell, D., Ed.; Academic: London, 1992; Vol. 27. (d) Hynes, J. T. In *Solvent Effects and Chemical Reactivity*; Bertràn, J., Tapia, O., Eds; Kluwer: Dordrecht, 1996.

(2) Truhlar, D. G.; Garrett, B. C.; Klippenstein, S. J. *J. Phys. Chem.* **1996**, *100*, 12771.

(3) (a) Bertrán, J. *Theor. Chem. Acc.* **1998**, *99*, 143. (b) Lim, D.; Jenson, C.; Repasky, M. P.; Jorgensen, W. L. *ACS Symp Ser.*, in press.

(4) (a) Storer, J. W.; Giesen, D. J.; Hawkins, G. D.; Lynch, G. C.; Cramer, C. J.; Truhlar, D. G. *ACS Symp. Ser.* **1994**, *568*, 24. (b) Gajewski, J. J.; Brichford, N. L. *ACS Symp. Ser.* **1994**, *568*, 243.

(5) (a) Dewar, M. J. S.; Douherty, R. C. *The PMO Theory of Organic Chemistry*; Plenum: New York, 1975; pp 274ff. (b) Garrett, B. C.; Schenter G. K. *ACS Symp. Ser.* **1994**, *568*, 122.

(6) Mezyk, S. P.; Bartels, D. M. *J. Phys. Chem.* **1994**, *98*, 10578.

(7) Truhlar, D. G.; Garrett, B. C. *Annu. Rev. Phys. Chem.* **1984**, *35*, 159.

(8) Truhlar, D. G.; Isaacson, A. D.; Garrett, B. C. In *Theory of Chemical Reaction Dynamics*; Baer, M., Ed.; CRC Press: Boca Raton, FL, 1985; Vol. 4, pp 65−137.

(9) Truhlar, D. G. In *The Reaction Path in Chemistry: Current Approaches and Perspectives*; Heidrich, D., Ed.; Kluwer: Dordrecht, The Netherlands, 1995; pp 229−255.

(10) (a) Lu, D.-h.; Truong, T. N.; Melissas, V. S.; Lynch, G. C.; Liu, Y.-P.; Garrett, B. C.; Steckler, R.; Isaacson, A. D.; Rai, S. N.; Hancock, G. C.; Lauderdale, J. G.; Joseph, T.; Truhlar, D. G. *Comput. Phys. Comm.* **1992**, *71*, 235. (b) Truhlar, D. G.; Lu, D.-h; Tucker, S. C.; Zhao, X. G.; Gonzalez-Lafont, A.; Truong, T. N.; Mavrie, D.; Liu, Y.-P.; Lynch, G. C. *ACS Symp. Series* **1992**, *502*, 16. (c) Truong, T. N.; Lu, D.-h.; Lynch, G. C.; Liu, Y.-P.; Melissas, V. S.; Stewart, J. J. P.; Steckler, R.; Garrett, B. C.; Isaacson, A. D.; González-Lafont, A.; Rai, S. N.; Hancock, G. C.; Joseph, T.; Truhlar, D. G. *Comput. Phys. Comm.* **1993**, *75*, 143. (d) Liu, Y.-P.; Lynch, G. C.; Truong, T. N.; Lu, D.-h.; Truhlar, D. G.; Garrett, B. C. *J. Am. Chem. Soc.* **1993**, *115*, 2408. (e) Liu, Y.-P.; Lu, D.-h.; Gonzalez-Lafont, A.; Truhlar, D. G.; Garrett, B. C. *J. Am. Chem. Soc.* **1993**, *115*, 7806.

(11) Kreevoy, M. M.; Truhlar, D. G. In *Investigation of Rates and Mechanisms of Reactions*, 4th ed.; Bernasconi, C. F., Ed.; Techniques of Chemistry, Vol. 6; John Wiley and Sons: New York, 1986; Part 1, pp 13−95.

(12) Garrett, B. C.; Schenter, G. K. *Int. Rev. Phys. Chem.* **1994**, *13*, 263.

(13) Truhlar, D. G.; Liu, Y.-P.; Schenter, G. K.; Garrett, B. C. *J. Phys. Chem.* **1994**, *98*, 8396.

(14) Chuang, Y.-Y.; Cramer, C. J.; Truhlar, D. G. *Int. J. Quantum Chem.* **1998**, *70*, 887.

(15) (a) Zhu, T.; Li, J.; Hawkins, G. D.; Cramer, C. J.; Truhlar, D. G. *J. Chem. Phys.* **1998**, *109*, 9117. (b) Li, J.; Hawkins, G. D.; Cramer, C. J.; Truhlar, D. G. *Chem. Phys. Lett.* **1998**, *288*, 293. (c) Li, J.; Zhu, T.; Hawkins, G. D.; Winget, P.; Liotard, D. A.; Cramer, C. J.; Truhlar, D. G. *Theor. Chem. Acc.*, in press.

(16) Zhu, Y.; Li, J.; Liotard, D. A.; Cramer, C. J.; Truhlar, D. G. *J. Chem. Phys.*, in press.

(17) Natanson, G. A.; Garrett, B. C.; Truong, T. N.; Joseph, J.; Truhlar, D. G. *J. Chem. Phys.* **1991**, *94*, 7875.

(18) Cramer, C. J.; Truhlar, D. G. In *Solute/Solvent Interactions*; Politzer, P., Murray, J. S., Ed.; Theoretical and Computational Chemistry, Vol. 1; Elsevier: Amsterdam, 1994; pp 9−54.

(19) King, P. M. In *Computer Simulation of Biomolecular Systems*; van Gunsteren, W. F., Weiner, P. K., Wilkinson, A. J., Eds.; ESCOM: Leiden, 1993; Vol. 2, p 267.

(20) Lendvay, G.; Bérces, T.; Márta, F. *J. Phys. Chem. A* **1997**, *101*, 1588.

(21) (a) Bauschlicher, C., Jr.; Langhoff, S. R.; Walch, S. P. *J. Chem. Phys.* **1992**, *96*, 450. (b) Bauschlicher, C., Jr.; Langhoff, S. R. *J. Chem. Phys.* **1990**, *173*, 367.

(22) Kolos, W.; Wolniewicz, L. *J. Chem. Phys.* **1964**, *41*, 3663.

(23) Tsang, W. *J. Phys. Chem. Ref. Data* **1987**, *16*, 471.

(24) (a) Melius, C. F. In *Chemistry and Physics of Energetic Materials*; Bulusu, S. N., Ed.; Kluwer Academic Publishers: Dordrecht, The Netherlands, 1990; pp 21−49. (b) Allendorf, M. D.; Melius, C. F. *J. Phys. Chem.* **1993**, *97*, 720. (c) Ho, P.; Melius, C. F. *J. Phys. Chem.* **1993**, *99*, 2166. (d) Zachariah, M. R.; Melius, C. F. *ACS Symp. Ser.* **1998**, *667*, 162.

(25) (a) Curtiss, L. A.; Raghavachari, K.; Trucks, G. W.; Pople, J. A. *J. Chem. Phys.* **1991**, *94*, 7221. (b) Curtiss, L. A.; Carpenter, J. E.; Raghavachari, K.; Pople, J. A. *J. Chem. Phys.* **1992**, *96*, 9030. (c) Curtiss, L. A.; Raghavachari, K.; Pople, J. A. *J. Chem. Phys.* **1993**, *98*, 1293.

Direct Dynamics for Free Radical Kinetics in Solution

J. Phys. Chem. A, Vol. 103, No. 25, 1999 **4909**

(26) (a) Hehre, W. J.; Radom, L.; Schleyer, P. v. R.; Pople, J. A. *Ab Initio Molecular Orbital Theory*; Wiley: New York, 1986. (b) Szabo, A.; Ostlund, N. S. *Modern Quantum Chemistry*; McGraw-Hill: New York, 1982.

(27) Møller, C.; Plesset, M. S. *Phys. Rev.* **1934**, *46*, 618.

(28) Pople, J. A.; Head-Gordon, M.; Raghavachari, K. *J. Chem. Phys.* **1987**, *87*, 5968.

(29) Purvis, G. D., III; Bartlett, R. J. *J. Chem. Phys.* **1982**, *76*, 1910.

(30) (a) Parr, R.; Yang, W. *Density-Functional Theory of Atoms and Moecules*; Oxford: New York, 1989. (b) Ziegler, T. *Chem. Rev.* **1991**, *91*, 651.

(31) (a) Becke, A. D. *J. Chem. Phys.* **1993**, *98*, 1372, 5648. (b) Stephens, P. J.; Devlin, F. J.; Chabalowski, C. F.; Frisch, M. J. *J. Phys. Chem.* **1994**, *98*, 11627.

(32) Baker, J.; Muir, M.; Andzelm, J.; Scheiner, A. *ACS Symp. Ser.* **1996**, *629*, 342.

(33) Kohn, W.; Becke, A. D.; Parr, R. G. *J. Am. Chem. Soc.* **1996**, *100*, 12974.

(34) Easton, R. E.; Giesen, D. J.; Welch, A.; Cramer, C. J.; Truhlar, D. G. *Theor. Chim. Acta* **1996**, *93*, 281.

(35) (a) Hehre, W. J.; Ditchfield, R.; Pople, J. A. *J. Chem. Phys.* **1972**, *56*, 2257. (b) Hariharan, P. C.; Pople, J. A. *Theor. Chim. Acta* **1973**, *28*, 213.

(36) Dunning, T. H. *J. Chem. Phys.* **1989**, *90*, 1007.

(37) (a) Hohenberg, P.; Kohn, W. *Phys. Rev.* **1964**, *136*, 13684. (b) Kohn, W.; Sham, L. J. *Phys. Rev.* **1965**, *140*, A1133. (c) Slater, J. C. *Quantum Theory of Molecules and Solids, Vol. 4: The Self-Consistent Field for Molecular and Solids*; McGraw-Hill: New York, 1974.

(38) Becke, A. D. *Phys. Rev. A.* **1988**, *38*, 3098.

(39) Perdew, J. P.; Wang, Y. *Phys. Rev. B* **1992**, *45*, 13244.

(40) Pitzer, K. S.; Gwinn, W. D. *J. Chem. Phys.* **1942**, *10*, 428.

(41) Pitzer, K. S. *J. Chem. Phys.* **1946**, *14*, 239.

(42) Truhlar, D. G. *J. Comput. Chem.* **1991**, *12*, 266.

(43) McQuarrie, D. A. *Statistical Mechanics*; Harper and Row: New York, 1973.

(44) Dewar, M. J.; Zoebisch, E. G.; Healy, E. F.; Stewart, J. J. *J. Am. Chem. Soc.* **1985**, *107*, 3902.

(45) (a) Gonzalez-Lafont, A.; Truong, T. N.; Truhlar, D. G. *J. Phys. Chem.* **1991**, *95*, 4618. (b) Liu, Y.-P.; Lu, D.-h.; Gonzalez-Lafont, A.; Truhlar, D. G. *J. Phys. Chem.* **1991**, *95*, 4618. (c) Rossi, I.; Truhlar, D. G. *Chem. Phys. Lett.* **1995**, *233*, 231.

(46) (a) Hehre, W. J.; Stewart, R. F.; Pople, J. A. *J. Chem. Phys.* **1969**, *51*, 2657. (b) Collins, J. B.; Schleyer, P. v. R.; Binkley, J. S.; Pople, J. A. *J. Chem. Phys.* **1976**, *64*, 5142.

(47) (a) Carroll, D. L. *AIAA J.* **1996**, *3*, 338. (b) The FORTRAN source code for the genetic algorithm can be obtained from D. L. Carroll's World Wide Web site at http://www.staff.uiuc.edu/~carroll/ga.html.

(48) Li, J.; Zhu, T.; Cramer, C. J.; Truhlar, D. G. *J. Phys. Chem. A* **1998**, *102*, 1820.

(49) Storer, J. W.; Giesen, D. J.; Cramer, C. J.; Truhlar, D. G. J. *Computer-Aided Mol. Des.* **1995**, *9*, 87.

(50) Storer, J. W.; Giesen, D. J.; Hawkins, G. D.; Lynch, G. C.; Cramer, C. J.; Truhlar, D. G.; Liotard, D. A. *ACS Symp. Ser.* **1994**, *568*, 24.

(51) Cramer, C. J.; Truhlar, D. G. *Chem. Phys. Lett.* **1992**, *198*, 74; **1993**, *202*, 567 (E).

(52) Hawkins, G. D.; Cramer, C. J.; Truhlar, D. G. *J. Phys. Chem. B* **1998**, *102*, 3257.

(53) Corchado, J. C.; Coitiño, E. L.; Chuang, Y.-Y.; Fast, P. L.; Truhlar, D. G. *J. Phys. Chem.* **1998**, *102*, 2424.

(54) Page, M.; McIver, J. W., Jr. *J. Chem. Phys.* **1988**, *88*, 922.

(55) (a) Jackels, C. F.; Gu, Z.; Truhlar, D. G. *J. Chem. Phys.* **1995**, *102*, 3188. (b) Nguyen, K. A.; Jackels, C. F.; Truhlar, D. G. *J. Chem. Phys.* **1996**, *104*, 6491. (c) Chuang, Y.-Y.; Truhlar, D. G. *J. Chem. Phys.* **1997**, *107*, 83. (d) Chuang, Y.-Y.; Truhlar, D. G. *J. Phys. Chem. A* **1998**, *102*, 242.

(56) Chuang, Y.-Y.; Corchado, J. C.; Truhlar, D. G. *J. Phys. Chem. A* **1999**, *103*, 1140.

(57) Villà, J.; Truhlar, D. G. *Theor. Chem. Acc.* **1997**, *97*, 317.

(58) Frisch, M. J.; Trucks, G. W.; Schlegel, H. B.; Gill, P. M. W.; Johnson, B. G.; Robb, M. A.; Cheeseman, J. R.; Keith, T.; Petersson, G. A.; Montgomery, J. A.; Raghavachari, K.; Al-Laham, M. A.; Zakrzewski, V. G.; Ortiz, J. V.; Foresman, J. B.; Cioslowski, J.; Stefanov, B. B.; Nanayakkara, A.; Challacombe, M.; Peng, C. Y.; Ayala, P. Y.; Chen, W.; Wong, M. W.; Andres, J. L.; Replogle, E. S.; Gomperts, R.; Martin, R. L.; Fox, D. J.; Binkley, J. S.; Defrees, D. J.; Baker, J.; Stewart, J. J. P.; Head-Gordon, M.; Gonzalez, C.; Pople, J. A. *Gaussian94*, Gaussian, Inc.; Pittsburgh, PA, 1995.

(59) Li, J.; Hawkins, G. D.; Liotard, D. A.; Cramer, C. J.; Truhlar, D. G. *mn-gsm98.2.3*; University of Minnesota: Minneapolis, 1998.

(60) Corchado, J.; Coitiño, E. L.; Chuang, Y.-Y.; Truhlar, D. G. *gaussrate8.0*; University of Minnesota: Minneapolis, 1998. Based on polyrate8.0 and Gaussian94.

(61) Chuang, Y.-Y.; Corchado, J. C.; Fast, P. L.; Villà, J.; Coitiño, E. L.; Hu, W.-P.; Liu Y.-P.; Lynch, G. C.; Nguyen, K.; Jackels, C. F.; Gu, M. Z.; Rossi, I.; Clayton, S.; Melissas, V.; Steckler, R.; Garrett, B. C.; Isaacson, A. D.; Truhlar, D. G. *polyrate8.1*; University of Minnesota: Minneapolis, 1999 [http://comp.chem.umn.edu/polyrate].

(62) Schmidt, M. W.; Baldridge, K. K.; Boatz, J. A.; Elbert, S. T.; Gordon, M. S.; Jensen, J. H.; Koseki, S.; Matsunaga, N.; Nguyen, K. A.; Su, S. J.; Windus, T. L.; Dupuis, M.; Montgomery, J. A. *J. Comput. Chem.* **1993**, *14*, 1347.

(63) Li, J.; Zhu, T.; Hawkins, G. D.; Chuang, Y.-Y.; Liotard, D. A.; Rinaldi, D.; Cramer C. J.; Truhlar, D. G. *gamesol2.1*; University of Minnesota: Minneapolis, 1999 [http://comp.chem.umn.edu/gamesol].

(64) Chuang, Y.-Y.; Corchado, J.; Truhlar, D. G. *gamesolrate8.1*; University of Minnesota: Minneapolis, 1999. Based on polyrate8.1 and gamesol2.1.

(65) Smaller, B.; Avery, E. C.; Remko, J. R. *J. Chem. Phys.* **1971**, *55*, 2414.

(66) Neta, P.; Fessenden, R. W.; Schuler, R. H. *J. Phys. Chem.* **1971**, *75*, 1654.

(67) Bartels, D. Personal communication.

(68) Tsang, W. Personal communication.

(69) Aders, W. K. In *Combust. Inst. European Symp.*; Weinberg, F., Ed.; Academic Press: London, 1973; Vol. 1, p 19.

(70) Meagher, J. F.; Kim, P.; Lee, J. H.; Timmons, R. B. *J. Phys. Chem.* **1974**, *78*, 2650.

(71) Lossack, A. M.; Roduner, E.; Bartels, D. M. *J. Phys. Chem. A* **1998**, *102*, 7462.

(72) Anbar, M.; Meyerstein, D. *J. Phys. Chem.* **1964**, *68*, 3184.

(73) Bunnett, J. F. In *Investigation of Rates and Mechanisms of Reactions*, 4th ed.; Bernasconi, C. F., Ed.; Techniques of Chemistry, Vol. 6; John Wiley and Sons: New York, 1986; Part I, pp 251–372.

(74) Truhlar, D. G. *J. Chem. Soc., Faraday Trans.* **1994**, *90*, 1740.

(75) Allison, T. C.; Truhlar, D. G. In *Modern Methods for Multidimensional Dynamics Computations in Chemistry*; Thompson, D. L., Ed.; World Scientific: Singapore, 1998; pp 618–712.